SIAM J. IMAGING SCIENCES
Vol. 7, No. 2, pp. 997–1034

Tensor Product Complex Tight Framelets with Increasing Directionality*

Bin Han† and Zhenpeng Zhao†

Abstract. Tensor product real-valued wavelets have been employed in many applications such as image processing with impressive performance. Edge singularities are ubiquitous and play a fundamental role in image processing and many other two-dimensional problems. Tensor product real-valued wavelets are known to be only suboptimal since they can only capture edges well along the coordinate axis directions (that is, the horizontal and vertical directions in dimension two). Among several approaches in the literature to enhance the performance of tensor product real-valued wavelets, the dual tree complex wavelet transform (DT-$\mathbb{C}$WT), proposed by Kingsbury [*Phil. Trans. R. Soc. Lond. A*, 357 (1999), pp. 2543–2560] and further developed by Selesnick, Baraniuk, and Kingsbury [*IEEE Signal Process. Mag.*, 22 (2005), pp. 123–151], is one of the most popular and successful enhancements of the classical tensor product real-valued wavelets by employing a correlated pair of orthogonal wavelet filter banks. The two-dimensional DT-$\mathbb{C}$WT is obtained essentially via tensor product and offers improved directionality with six directions. In this paper we shall further enhance the performance of the DT-$\mathbb{C}$WT for the problem of image denoising. Using a framelet-based approach and the notion of discrete affine systems, we shall propose a family of tensor product complex tight framelets TP-$\mathbb{C}$TF$_n$ for all integers $n \geq 3$ with increasing directionality, where n refers to the number of filters in the underlying one-dimensional complex tight framelet filter bank. For dimension two, such a tensor product complex tight framelet TP-$\mathbb{C}$TF$_n$ offers $\frac{1}{2}(n-1)(n-3)+4$ directions when n is odd and $\frac{1}{2}(n-4)(n+2)+6$ directions when n is even. In particular, we shall show that TP-$\mathbb{C}$TF$_4$, which is different from the DT-$\mathbb{C}$WT in both nature and design, provides an alternative to the DT-$\mathbb{C}$WT. Indeed, we shall see that TP-$\mathbb{C}$TF$_4$ behaves quite similar to the DT-$\mathbb{C}$WT by offering six directions in dimension two, employing the tensor product structure, and enjoying slightly less redundancy than the DT-$\mathbb{C}$WT. Then we shall apply TP-$\mathbb{C}$TF$_n$ to the problem of image denoising. We shall see that the performance of TP-$\mathbb{C}$TF$_4$ for image denoising is comparable to that of the DT-$\mathbb{C}$WT. Better results on image denoising can be obtained by using other TP-$\mathbb{C}$TF$_n$, for example, $n = 6$, which has 14 directions in dimension two. Moreover, TP-$\mathbb{C}$TF$_n$ allows us to further improve the DT-$\mathbb{C}$WT by using TP-$\mathbb{C}$TF$_n$ as the first stage filter bank in the DT-$\mathbb{C}$WT. We shall also provide discussion and comparison of TP-$\mathbb{C}$TF$_n$ with several generalizations of the DT-$\mathbb{C}$WT, shearlets, and directional nonseparable tight framelets.

Key words. complex tight framelet filter banks, directionality, dual tree complex wavelet transform, tensor product, image denoising

AMS subject classifications. 42C40, 42C15, 65T60, 94A08

DOI. 10.1137/130928558

1. Introduction and motivations.

In this paper we shall take a framelet-based approach to enhance the performance of the classical tensor product real-valued wavelets by providing a family of tensor product complex tight framelet filter banks with increasing directionality.

*Received by the editors July 11, 2013; accepted for publication (in revised form) February 24, 2014; published electronically May 15, 2014. This work was supported in part by the Natural Sciences and Engineering Research Council of Canada (NSERC Canada) under grant RGP 228051.
http://www.siam.org/journals/siims/7-2/92855.html
†Department of Mathematical and Statistical Sciences, University of Alberta, Edmonton, AB T6G 2G1, Canada (bhan@ualberta.ca, http://www.ualberta.ca/∼bhan, zzhao7@ualberta.ca).

On the other hand, we provide alternatives and improvements to the well-known dual tree complex wavelet transform (DT-$\mathbb{C}$WT), which has been proposed by Kingsbury in [24, 25] and further developed by Selesnick, Baraniuk, and Kingsbury in [34]. Then we shall apply the constructed tensor product complex tight framelets for the problem of image denoising.

To explain our motivations, let us first recall some definitions. By $l_2(\mathbb{Z}^d)$ we denote the space of all complex-valued sequences $u = \{u(k)\}_{k\in\mathbb{Z}^d} : \mathbb{Z}^d \to \mathbb{C}$ such that $\|u\|_{l_2(\mathbb{Z}^d)} := (\sum_{k\in\mathbb{Z}^d} |u(k)|^2)^{1/2} < \infty$. The Fourier series (or symbol) of a sequence $u \in l_2(\mathbb{Z}^d)$ is defined to be $\widehat{u}(\xi) := \sum_{k\in\mathbb{Z}^d} u(k)e^{-ik\cdot\xi}, \xi \in \mathbb{R}^d$, which is a $2\pi\mathbb{Z}^d$-periodic measurable function in $L_2(\mathbb{T}^d)$ such that $\|\widehat{u}\|^2_{L_2(\mathbb{T}^d)} := \frac{1}{(2\pi)^d}\int_{[-\pi,\pi)^d} |\widehat{u}(\xi)|^2 d\xi = \|u\|^2_{l_2(\mathbb{Z}^d)} = \sum_{k\in\mathbb{Z}^d} |u(k)|^2 < \infty$. If $u \in l_1(\mathbb{Z}^d)$, that is, $\|u\|_{l_1(\mathbb{Z}^d)} := \sum_{k\in\mathbb{Z}^d} |u(k)| < \infty$, then $u \in l_2(\mathbb{Z}^d)$ and $\widehat{u} \in C(\mathbb{T}^d)$ is a continuous function.

For filters $a, b_1, \ldots, b_s \in l_1(\mathbb{Z}^d)$, $\{a; b_1, \ldots, b_s\}$ is called a d-dimensional (dyadic) tight framelet filter bank if

$$|\widehat{a}(\xi)|^2 + \sum_{\ell=1}^{s} |\widehat{b_\ell}(\xi)|^2 = 1, \tag{1.1}$$

$$\widehat{a}(\xi)\overline{\widehat{a}(\xi+\pi\omega)} + \sum_{\ell=1}^{s} \widehat{b_\ell}(\xi)\overline{\widehat{b_\ell}(\xi+\pi\omega)} = 0 \qquad \forall\, \omega \in \Omega\backslash\{0\} \tag{1.2}$$

for all $\xi \in \mathbb{R}^d$, where $\Omega := [0,1]^d \cap \mathbb{Z}^d$. The filter a is called a low-pass filter since we often require $\widehat{a}(0) = 1$, and all the filters $b_1, \ldots, b_s$ are called high-pass filters since we often have $\widehat{b_1}(0) = \cdots = \widehat{b_s}(0) = 0$. Note that if $\widehat{a}(0) = 1$ in a tight framelet filter bank $\{a; b_1, \ldots, b_s\}$, then it follows directly from (1.1) that $\widehat{b_1}(0) = \cdots = \widehat{b_s}(0) = 0$. When $s = 2^d - 1$, a d-dimensional (dyadic) tight framelet filter bank $\{a; b_1, \ldots, b_{2^d-1}\}$ is called a d-dimensional (dyadic) orthogonal wavelet filter bank. Let $\{a; b_1, \ldots, b_s\}$ be a d-dimensional tight framelet filter bank. Under the mild condition $|1-\widehat{a}(\xi)| \le C|\xi|^\tau, \xi \in [-\pi,\pi]^d$ for some positive numbers C and τ (all our tight framelet filter banks constructed in this paper satisfy this condition with $\tau = 1$), the function $\widehat{\phi}(\xi) := \prod_{j=1}^{\infty} \widehat{a}(2^{-j}\xi)$ is a well-defined function in $L_2(\mathbb{R}^d)$ and $\{\phi; \psi^1, \ldots, \psi^s\}$ is a tight framelet in $L_2(\mathbb{R}^d)$; that is, the affine system

$$\mathsf{AS}_0(\phi; \psi^1, \ldots, \psi^s) := \{\phi(\cdot - k) \,:\, k \in \mathbb{Z}^d\} \cup \{2^{dj/2}\psi^\ell(2^j\cdot - k) \,:\, k \in \mathbb{Z}^d, j \in \mathbb{N}\cup\{0\}, \ell = 1, \ldots, s\}$$

is a (normalized) tight frame for $L_2(\mathbb{R}^d)$ satisfying

$$\|f\|^2_{L_2(\mathbb{R}^d)} = \sum_{k\in\mathbb{Z}^d} |\langle f, \phi(\cdot - k)\rangle|^2 + \sum_{j=0}^{\infty}\sum_{\ell=1}^{s}\sum_{k\in\mathbb{Z}^d} |\langle f, 2^{dj/2}\psi^\ell(2^j\cdot - k)\rangle|^2 \qquad \forall\, f \in L_2(\mathbb{R}^d),$$

where the functions $\psi^1, \ldots, \psi^s$ are defined by $\widehat{\psi^\ell}(\xi) := \widehat{b_\ell}(\xi/2)\widehat{\phi}(\xi/2)$, $\ell = 1, \ldots, s$. $\{\phi; \psi^1, \ldots, \psi^s\}$ is called an orthonormal wavelet in $L_2(\mathbb{R}^d)$ if $s = 2^d - 1$ and $\mathsf{AS}_0(\phi; \psi^1, \ldots, \psi^s)$ is an orthonormal basis for $L_2(\mathbb{R}^d)$. Throughout this paper, the word framelet is a synonym for frame wavelet. For more details on tight framelets and their applications, see [3, 5, 6, 13, 18, 20, 21, 22, 31, 32, 37] and many references therein. Due to this connection between a tight framelet filter bank and a tight framelet in the function space $L_2(\mathbb{R}^d)$, we shall concentrate

on tight framelet filter banks instead of tight framelets in $L_2(\mathbb{R}^d)$ in this paper. In fact, to understand the properties and performance of the discrete framelet or wavelet transform, it is more important to study its underlying discrete affine systems $\mathsf{DAS}_J(\{a; b_1, \dots, b_s\})$ than its associated functional affine system $\mathsf{AS}_0(\phi; \psi^1, \dots, \psi^s)$ in $L_2(\mathbb{R}^d)$. See [19] for more details on discrete affine systems, and see [18] for the natural correspondence between functional affine systems and filter banks.

The simplest way to obtain a d-dimensional tight framelet filter bank is to use tensor product of one-dimensional tight framelet filter banks. For simplicity of presentation, in this paper we discuss only tensor product for dimension two. For two one-dimensional filters $u, v \in l_1(\mathbb{Z})$, their tensor product filter $u \otimes v$ in dimension two is simply defined to be $[u \otimes v](j,k) = u(j)v(k)$, $j,k \in \mathbb{Z}$. Let $\{a; b_1, \dots, b_s\}$ be a one-dimensional tight framelet filter bank. Then its tensor product tight framelet filter bank in dimension two is given by $\{a; b_1, \dots, b_s\} \otimes \{a; b_1, \dots, b_s\}$. More explicitly,

$$\{a \otimes a\} \cup \{a \otimes b_1, \dots, a \otimes b_s\} \cup \{b_1 \otimes a, \dots, b_s \otimes a\} \cup \{b_\ell \otimes b_m \ : \ \ell, m = 1, \dots, s\},$$

where $a \otimes a$ is the low-pass filter and all other filters above are high-pass filters. It is well known in the literature [2, 7, 10, 18, 24, 25, 27, 33, 34] that tensor product real-valued wavelets or framelets lack directionality. To see this point well, let us look at the simplest example of the tensor product Haar orthogonal wavelet filter bank in dimension two. The one-dimensional Haar orthogonal wavelet filter bank $\{a; b\}$ is given by $a = \{\frac{1}{2}, \frac{1}{2}\}_{[0,1]}$ and $b = \{\frac{1}{2}, -\frac{1}{2}\}_{[0,1]}$. Then $\{a \otimes a; a \otimes b, b \otimes a, b \otimes b\}$ is a two-dimensional real-valued orthogonal wavelet filter bank, where

$$\begin{aligned} a \otimes a &= \begin{bmatrix} \frac{1}{4} & \frac{1}{4} \\ \frac{1}{4} & \frac{1}{4} \end{bmatrix}_{[0,1]^2}, \quad a \otimes b = \begin{bmatrix} -\frac{1}{4} & -\frac{1}{4} \\ \frac{1}{4} & \frac{1}{4} \end{bmatrix}_{[0,1]^2}, \\ b \otimes a &= \begin{bmatrix} \frac{1}{4} & -\frac{1}{4} \\ \frac{1}{4} & -\frac{1}{4} \end{bmatrix}_{[0,1]^2}, \quad b \otimes b = \begin{bmatrix} -\frac{1}{4} & \frac{1}{4} \\ \frac{1}{4} & -\frac{1}{4} \end{bmatrix}_{[0,1]^2}. \end{aligned} \tag{1.3}$$

Note that $a \otimes b$ has horizontal direction and $b \otimes a$ has vertical direction, but $b \otimes b$ does not exhibit any directionality (instead, $b \otimes b$ is sort of a saddle point) and is known as the checkerboard problem in the literature. On the other hand, it is widely known (see [2, 7, 10, 24, 27, 34] and many references therein) that edge singularities are ubiquitous and play a fundamental role in many two-dimensional problems such as image processing. To enhance the performance of tensor product real-valued wavelets by improving directionality, several approaches have been proposed in the literature. For example, the curvelet transform [2] and the shearlet transform [22, 26, 27, 28] for dimension two on $\mathbb{R}^2$, steerable filter banks [10] and contourlets [7] in the discrete domain $\mathbb{Z}^2$, symmetric complex orthogonal wavelet filter banks [15, 16, 29], the DT-$\mathbb{C}$WT in [24, 25, 33, 34, 35, 36], etc.

Among all these approaches, the DT-$\mathbb{C}$WT is probably one of the most popular and successful approaches to improving the performance of the classical tensor product real-valued wavelet transform. The success of the DT-$\mathbb{C}$WT largely lies in three major advantages of the DT-$\mathbb{C}$WT: (i) The two-dimensional DT-$\mathbb{C}$WT offers six directions (roughly along $\pm 15^\circ$, $\pm 45^\circ$, $\pm 75^\circ$), in comparison with only two directions (that is, horizontal and vertical directions)

of classical tensor product real-valued wavelets. (ii) The DT-$\mathbb{C}$WT is nearly shift-invariant without high redundancy, comparing with the shift-invariant undecimated wavelet transform. (iii) The d-dimensional DT-$\mathbb{C}$WT can be implemented by applying 2^d tensor product discrete orthogonal wavelet transforms in parallel. Since we shall adopt the filter bank approach and preserve the tensor product structure, we shall discuss the DT-$\mathbb{C}$WT in detail in this paper. Our goal of this paper is to provide alternatives and further improvements of the DT-$\mathbb{C}$WT.

To understand the key features and advantages of the DT-$\mathbb{C}$WT, let us first look at the possible shortcomings of tensor product real-valued filters. For a one-dimensional filter $u : \mathbb{Z} \to \mathbb{C}$, it is straightforward to see that u is a real-valued filter (that is, $u : \mathbb{Z} \to \mathbb{R}$) if and only if $\overline{\widehat{u}(\xi)} = \widehat{u}(-\xi)$. Therefore, for a real-valued filter u, we always have $|\widehat{u}(-\xi)| = |\widehat{u}(\xi)|$ and the magnitude of its frequency spectrum is symmetric about the origin. If both u and v are one-dimensional real-valued high-pass filters satisfying $\widehat{u}(0) = \widehat{v}(0) = 0$, since the magnitudes of the frequency spectrums of u and v are symmetric about the origin, it is easy to see that the frequency spectrum of the two-dimensional real-valued tensor product filter $u \otimes v$ concentrates equally in the four quadrants (more precisely, the four corners) of the basic frequency square $[-\pi, \pi]^2$. Consequently, the filter $u \otimes v$ lacks directionality and behaves like a saddle point, just as the tensor product filter $b \otimes b$ in (1.3) in the two-dimensional tensor product Haar orthogonal wavelet filter bank. The same argument applies to tensor product real-valued functions. To achieve directionality while preserving the tensor product structure, as argued in [24, 25, 33, 34] and many other papers, it is natural to consider complex-valued high-pass filters u and v so that the frequency spectrums of u and v largely lie on either $[0, \pi)$ or $(-\pi, 0]$. The DT-$\mathbb{C}$WT achieves this goal by having the analyticity property of the complex wavelets (see [24, 25, 33, 34]) through a pair of correlated real-valued orthogonal wavelets $\{\phi^1; \psi^1\}$ and $\{\phi^2; \psi^2\}$ such that (ψ^1, ψ^2) forms an approximate Hilbert-transform pair:

$$\widehat{\psi^2}(\xi) \approx -i \operatorname{sgn}(\xi) \widehat{\psi^1}(\xi), \qquad \xi \in \mathbb{R}, \tag{1.4}$$

where $\operatorname{sgn}(\xi) = 1$ if $\xi \geq 0$, and -1 otherwise. To better understand the DT-$\mathbb{C}$WT, we shall study the key ingredients of the DT-$\mathbb{C}$WT in section 2 using the framework of discrete affine systems, which have been introduced in [19].

As demonstrated in many interesting works by the research groups of Kingsbury in [24, 25] and Selesnick and co-workers in [33, 34, 35, 36], the DT-$\mathbb{C}$WT has impressive performance over the classical tensor product real-valued wavelets, for example, in image denoising in [24, 35, 36] and many references therein. However, using dyadic orthogonal wavelet filter banks and the Hilbert transform, to the best of our knowledge, it is not easy to generalize the DT-$\mathbb{C}$WT to have more directions. To improve DT-$\mathbb{C}$WT-like transforms, [38] proposed an approach which is closely related to the steerable pyramid transform in [10] and uses an extension of the Hilbert transform to higher dimensions. In this paper, we shall adopt a framelet-based approach and use discrete affine systems to provide alternatives and improvements to the DT-$\mathbb{C}$WT. This framelet-based approach allows us to achieve improved directionality while avoiding the use of the Hilbert transform. At the end of this paper, we shall also discuss and compare our framelet-based approach with generalizations of the DT-$\mathbb{C}$WT in [1, 4].

The structure of the paper is as follows. In order to understand the performance of the discrete wavelet transform and the DT-$\mathbb{C}$WT, we shall first recall from [19] the notion of

discrete affine systems associated with the multilevel discrete wavelet or framelet transform. Then we shall discuss and analyze the main features of the DT-$\mathbb{C}$WT under the framework of discrete affine systems. The notion of discrete affine systems also plays a key role in our understanding and construction of tensor product complex tight framelet filter banks in section 4. For application of the DT-$\mathbb{C}$WT to image denoising, we shall demonstrate in section 3 that the DT-$\mathbb{C}$WT, employing a pair of frequency-based (that is, bandlimited) correlated orthogonal wavelet filter banks, performs equally well as the original DT-$\mathbb{C}$WT employing a pair of finitely supported correlated orthogonal wavelet filter banks proposed and used in [24, 25, 34, 36]. In section 4, we shall introduce and construct a family of tensor product complex tight framelets TP-$\mathbb{C}$TF$_n$ with $n \geq 3$, where n refers to the number of filters in the underlying one-dimensional complex tight framelet filter banks. Such a tensor product complex tight framelet TP-$\mathbb{C}$TF$_n$ offers $\frac{1}{2}(n-1)(n-3)+4$ directions when n is odd and $\frac{1}{2}(n-4)(n+2)+6$ directions when n is even. In section 4, we shall show that TP-$\mathbb{C}$TF$_4$, which is different from the DT-$\mathbb{C}$WT in both nature and design, provides an alternative to the DT-$\mathbb{C}$WT. Indeed, we shall see that TP-$\mathbb{C}$TF$_4$ behaves quite similar to the DT-$\mathbb{C}$WT: TP-$\mathbb{C}$TF$_4$ offers six directions in dimension two, employs the tensor product structure, and has slightly less redundancy than the DT-$\mathbb{C}$WT by using only one low-pass filter in TP-$\mathbb{C}$TF$_4$ instead of four low-pass filters in the DT-$\mathbb{C}$WT for dimension two. When TP-$\mathbb{C}$TF$_4$ is applied to the problem of image denoising, its performance is comparable to the DT-$\mathbb{C}$WT. Moreover, we shall demonstrate in section 4 that better results on image denoising, in terms of PSNR, can be obtained by using other TP-$\mathbb{C}$TF$_n$, for example, $n = 6$, which has 14 directions in dimension two. Experiments on image denoising using TP-$\mathbb{C}$TF$_n$ and detailed comparison with the DT-$\mathbb{C}$WT will be provided in section 4. Then we shall discuss in section 5 the choice of the initial filter banks for the first level of the DT-$\mathbb{C}$WT for further improvements. We shall show that TP-$\mathbb{C}$TF$_n$ allows us to further improve the DT-$\mathbb{C}$WT by using TP-$\mathbb{C}$TF$_n$ as the first stage filter bank in the DT-$\mathbb{C}$WT. In section 6, we shall discuss and compare our proposed TP-$\mathbb{C}$TF$_n$ with other recent developments on the DT-$\mathbb{C}$WT and wavelet analysis such as the dual tree complex wavelet packet transform [1] and the M-band DT-$\mathbb{C}$WT [4], shearlets [8, 9, 12, 22, 26, 27, 28], and directional nonseparable tight framelets [18]. We shall also compare the performance of TP-$\mathbb{C}$TF$_n$ with the image denoising results by shearlets reported in [27, 28]. Finally, we shall summarize the main features of TP-$\mathbb{C}$TF$_n$ in section 6 for possible further improvements.

2. Understand the DT-$\mathbb{C}$WT using discrete affine systems. Wavelets and framelets have been extensively studied in the continuum domain. To understand the performance of the classical discrete wavelet transform and the DT-$\mathbb{C}$WT, it is of fundamental importance to study the discrete wavelet or framelet transform directly. For this purpose, in this section we shall first recall the notion of discrete affine systems associated with the discrete wavelet transform or any discrete linear transform. Then we shall investigate the key features of the DT-$\mathbb{C}$WT under the framework of discrete affine systems.

The DT-$\mathbb{C}$WT has been extensively studied and discussed in [1, 4, 24, 25, 33, 34, 35, 36] and many other references in the setting of filter banks and functions in $L_2(\mathbb{R})$ (that is, refinable functions and wavelet functions in $L_2(\mathbb{R})$). Our discussion on the DT-$\mathbb{C}$WT in this section through the notion of discrete affine systems provides complementary and probably

more direct understanding of the DT-ℂWT. Our investigation of the DT-ℂWT in this section by using discrete affine systems also allows us to see and better understand the advantages and possible places for further improvements of the DT-ℂWT.

2.1. The multilevel discrete framelet transform and discrete affine systems. Let us first recall the multilevel discrete framelet transform using a d-dimensional tight framelet filter bank $\{a; b_1, \ldots, b_s\}$. For a positive integer J and an input signal $v \in l_2(\mathbb{Z}^d)$, a J-level discrete framelet decomposition computes the framelet/wavelet coefficients $v_j, w_{\ell,j}$ through the following recursive formulas:

$$v_j := 2^{-d/2}\mathcal{T}_a v_{j-1}, \quad w_{\ell,j} := 2^{-d/2}\mathcal{T}_{b_\ell} v_{j-1}, \qquad \ell = 1, \ldots, s,\ j = 1, \ldots, J,$$

where $v_0 = v$ is the input signal and the transition operator $\mathcal{T}_a : l_2(\mathbb{Z}^d) \to l_2(\mathbb{Z}^d)$ is defined to be

$$[\mathcal{T}_a v](n) = 2^d \sum_{k\in\mathbb{Z}^d} v(k)\overline{a(k-2n)}, \qquad n \in \mathbb{Z}^d.$$

A J-level discrete framelet reconstruction is used to recursively reconstruct the original signal as follows:

$$\mathring{v}_{j-1} := 2^{-d/2}\mathcal{S}_a \mathring{v}_j + 2^{-d/2}\sum_{\ell=1}^{s} \mathcal{S}_{b_\ell}\mathring{w}_{\ell,j}, \qquad j = J, \ldots, 1,$$

where the subdivision operator $\mathcal{S}_a : l_2(\mathbb{Z}^d) \to l_2(\mathbb{Z}^d)$ is defined to be

$$[\mathcal{S}_a v](n) = 2^d \sum_{k\in\mathbb{Z}^d} v(k)a(n-2k), \qquad n \in \mathbb{Z}^d.$$

Using convolution, upsampling, and downsampling, we see that $\mathcal{T}_a v = 2^d(v * a^\star)\downarrow 2I_d$ and $\mathcal{S}_a v = 2^d(v \uparrow 2I_d) * a$, where the adjoint filter $a^\star$ is defined by $a^\star(k) := \overline{a(-k)}$, $k \in \mathbb{Z}^d$, or equivalently, $\widehat{a^\star}(\xi) := \overline{\widehat{a}(\xi)}$. See Figure 1 for an illustration of the one-dimensional 2-level discrete framelet transform.

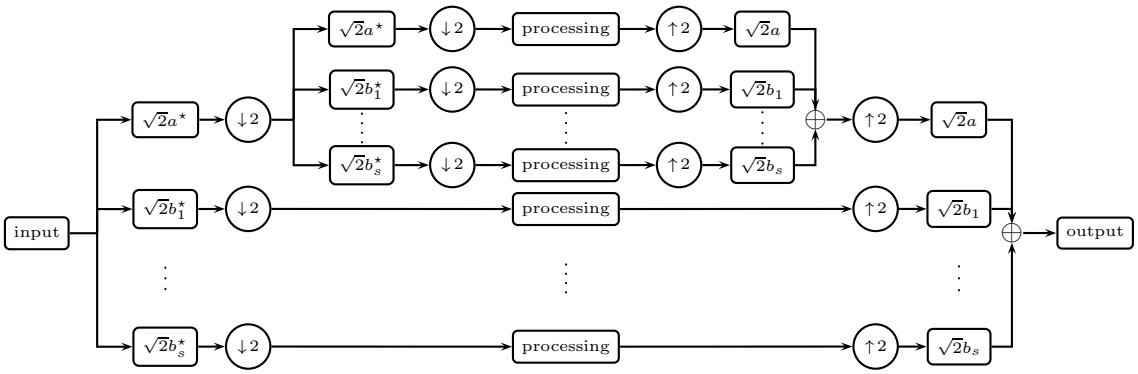

Figure 1. *Diagram of the one-dimensional two-level discrete framelet transform using a one-dimensional tight framelet filter bank $\{a; b_1, \ldots, b_s\}$. Here each box with a filter inside it means convolution with the filter inside the box. Note that $\mathcal{T}_a v = 2(v * a^\star)\downarrow 2$ and $\mathcal{S}_a v = 2(v\uparrow 2) * a$.*

Following [19], we define multilevel filters a_j and $b_{\ell,j}$ with $j \in \mathbb{N}$ and $\ell = 1, \ldots, s$ by

$$\begin{aligned} \widehat{a_j}(\xi) &:= 2^{dj/2}\widehat{a}(\xi)\widehat{a}(2\xi)\cdots\widehat{a}(2^{j-2}\xi)\widehat{a}(2^{j-1}\xi) \quad \text{and} \\ \widehat{b_{\ell,j}}(\xi) &:= 2^{dj/2}\widehat{a}(\xi)\widehat{a}(2\xi)\cdots\widehat{a}(2^{j-2}\xi)\widehat{b_\ell}(2^{j-1}\xi). \end{aligned} \tag{2.1}$$

Note that $a_1 = 2^{d/2}a$ and $b_{\ell,1} = 2^{d/2}b_\ell$. Now we define

$$a_{j;k} := a_j(\cdot - 2^j k), \quad b_{\ell,j;k} := b_{\ell,j}(\cdot - 2^j k), \qquad k \in \mathbb{Z}^d, j \in \mathbb{N}. \tag{2.2}$$

Note that $l_2(\mathbb{Z}^d)$ is a Hilbert space equipped with the inner product $\langle v, w\rangle = \sum_{k\in\mathbb{Z}^d} v(k)\overline{w(k)}$. As shown in [19], we have

$$v_j(k) = \langle v, a_{j;k}\rangle \quad \text{and} \quad w_{\ell,j}(k) = \langle v, b_{\ell,j;k}\rangle, \qquad k \in \mathbb{Z}^d,\ j \in \mathbb{N},\ \ell = 1, \ldots, s.$$

Consequently, the J-level discrete framelet transform is exactly to compute the following representation:

$$v = \sum_{k\in\mathbb{Z}^d} \langle v, a_{J;k}\rangle a_{J;k} + \sum_{j=1}^{J}\sum_{\ell=1}^{s}\sum_{k\in\mathbb{Z}^d} \langle v, b_{\ell,j;k}\rangle b_{\ell,j;k} \qquad \forall\, v \in l_2(\mathbb{Z}^d) \tag{2.3}$$

with the series converging unconditionally in $l_2(\mathbb{Z}^d)$. Moreover, we have the following cascade structure on which the fast multilevel discrete framelet transform is based:

$$\sum_{k\in\mathbb{Z}^d} \langle v, a_{j-1;k}\rangle a_{j-1;k} = \sum_{k\in\mathbb{Z}^d} \langle v, a_{j;k}\rangle a_{j;k} + \sum_{\ell=1}^{s}\sum_{k\in\mathbb{Z}^d} \langle v, b_{\ell,j;k}\rangle b_{\ell,j;k} \qquad \forall\, v \in l_2(\mathbb{Z}^d), j \in \mathbb{N}.$$

Following [19], for every positive integer $J \in \mathbb{N}$, we define a J-level discrete affine system associated with the filter bank $\{a; b_1, \ldots, b_s\}$ by

$$\mathsf{DAS}_J(\{a; b_1, \ldots, b_s\}) := \{a_{J;k} \,:\, k \in \mathbb{Z}^d\} \cup \bigcup_{j=1}^{J} \{b_{\ell,j;k} \,:\, k \in \mathbb{Z}^d, \ell = 1, \ldots, s\}. \tag{2.4}$$

It is not difficult to directly verify [19] that $\{a; b_1, \ldots, b_s\}$ is a tight framelet filter bank if and only if $\mathsf{DAS}_J(\{a; b_1, \ldots, b_s\})$ is a (normalized) tight frame for $l_2(\mathbb{Z}^d)$ for every integer $J \in \mathbb{N}$, that is,

$$\|v\|^2_{l_2(\mathbb{Z}^d)} = \sum_{u\in\mathsf{DAS}_J(\{a;b_1,\ldots,b_s\})} |\langle v, u\rangle|^2 \qquad \forall\, v \in l_2(\mathbb{Z}^d),$$

which leads directly to the discrete representation in (2.3). Similarly, $\{a; b_1, \ldots, b_{2^d-1}\}$ is an orthogonal wavelet filter bank if and only if $\mathsf{DAS}_J(\{a; b_1, \ldots, b_{2^d-1}\})$ is an orthonormal basis for $l_2(\mathbb{Z}^d)$ for every $J \in \mathbb{N}$. Therefore, the performance of the multilevel discrete framelet transform completely depends on its underlying discrete affine systems. We now present an example to illustrate the generators in a discrete affine system. Let $\{a; b\}$ be the Daubechies orthogonal wavelet filter bank given by

$$a = \left\{\tfrac{1+\sqrt{3}}{8}, \tfrac{3+\sqrt{3}}{8}, \tfrac{3-\sqrt{3}}{8}, \tfrac{1-\sqrt{3}}{8}\right\}_{[-1,2]}, \qquad b = \left\{\tfrac{1-\sqrt{3}}{8}, \tfrac{\sqrt{3}-3}{8}, \tfrac{3+\sqrt{3}}{8}, -\tfrac{1+\sqrt{3}}{8}\right\}_{[-1,2]}. \tag{2.5}$$

Some generators of the discrete affine systems $\mathsf{DAS}_J(\{a; b\})$ are presented in Figure 2.

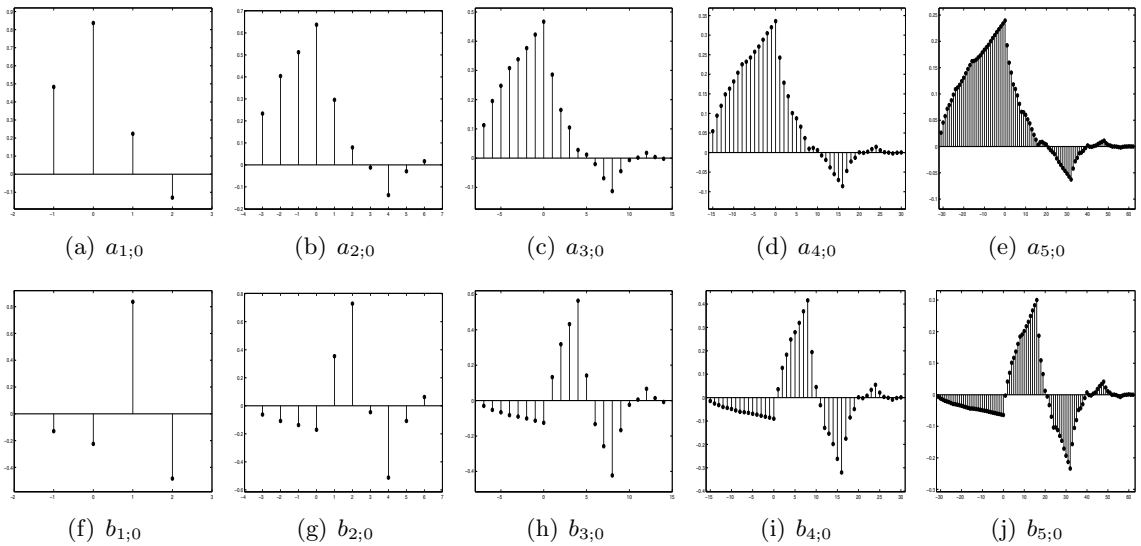

(a) $a_{1;0}$ (b) $a_{2;0}$ (c) $a_{3;0}$ (d) $a_{4;0}$ (e) $a_{5;0}$

(f) $b_{1;0}$ (g) $b_{2;0}$ (h) $b_{3;0}$ (i) $b_{4;0}$ (j) $b_{5;0}$

Figure 2. *Some generators of the one-dimensional discrete affine systems* $\mathsf{DAS}_J(\{a;b\})$ *with* $J = 1, \ldots, 5$ *and the Daubechies orthogonal wavelet filter bank* $\{a;b\}$ *in* (2.5).

2.2. Discrete affine systems for the one-dimensional DT-ℂWT. To discuss the key features of the DT-ℂWT using discrete affine systems, in the following let us first recall a one-dimensional orthogonal wavelet filter bank $\{a;b\}$, that is, a tight framelet filter bank with only one high-pass filter. More explicitly, for filters $a, b \in l_1(\mathbb{Z})$, $\{a;b\}$ is an orthogonal wavelet filter bank if

$$\begin{bmatrix} \widehat{a}(\xi) & \widehat{b}(\xi) \\ \widehat{a}(\xi+\pi) & \widehat{b}(\xi+\pi) \end{bmatrix} \begin{bmatrix} \overline{\widehat{a}(\xi)} & \overline{\widehat{a}(\xi+\pi)} \\ \overline{\widehat{b}(\xi)} & \overline{\widehat{b}(\xi+\pi)} \end{bmatrix} = \begin{bmatrix} 1 & 0 \\ 0 & 1 \end{bmatrix}. \tag{2.6}$$

We often call a a low-pass filter and b a high-pass filter. It is easy to see that the low-pass filter a in an orthogonal wavelet filter bank $\{a;b\}$ must be an orthogonal filter satisfying $|\widehat{a}(\xi)|^2 + |\widehat{a}(\xi+\pi)|^2 = 1$, and the high-pass filter b is almost uniquely obtained from the orthogonal low-pass filter a through the relation

$$\widehat{b}(\xi) = e^{-i\xi}\overline{\widehat{a}(\xi+\pi)}. \tag{2.7}$$

In this paper, we always assume that the high-pass filter b in a one-dimensional orthogonal wavelet filter bank $\{a;b\}$ is always obtained from an orthogonal low-pass filter a through the relation in (2.7).

In the following, we discuss some key features of the DT-ℂWT using discrete affine systems. As discussed in [24, 25, 33, 34], the DT-ℂWT employs three sets of real-valued orthogonal wavelet filter banks: $\{a^0;b^0\}$ and a correlated pair $\{a^1;b^1\}$ and $\{a^2,b^2\}$. The initial filter bank $\{a^0;b^0\}$ can be any real-valued orthogonal wavelet filter bank and is used for the first level/stage in the DT-ℂWT. Due to the constraint on an approximate Hilbert-transform pair in (1.4), the pair of correlated real-valued orthogonal wavelet filter banks $\{a^1;b^1\}$ and $\{a^2;b^2\}$ are linked to each other through the half-shift condition (see [24, 25, 33, 34]):

$$\widehat{a^2}(\xi) \approx e^{i\theta(\xi)}\widehat{a^1}(\xi) \qquad \text{with} \qquad \theta(\xi) := -\xi/2 + \pi\lfloor \tfrac{\xi+\pi}{2\pi} \rfloor, \qquad \xi \in \mathbb{R}, \tag{2.8}$$

where $\lfloor \cdot \rfloor$ is the floor function such that $\lfloor x \rfloor = n$ for $n \le x < n+1$ with n being an integer. Note that $e^{i\theta(\xi)}$ is 2π-periodic and the phase function $\theta(\xi) = -\xi/2$ for $\xi \in [-\pi, \pi)$, which corresponds to (approximate) half-shift in the discrete time domain $\mathbb{Z}$. That is, the half-shift condition is equivalent to saying that $a^2 \approx a^1(\cdot - 1/2)$, which should be interpreted properly since both filters a^1 and a^2 are defined only on $\mathbb{Z}$. The pair of correlated real-valued orthogonal wavelet filter banks $\{a^1; b^1\}$ and $\{a^2; b^2\}$ is used for all other levels/stages except the first level in the DT-$\mathbb{C}$WT. The half-shift condition in (2.8) induces relations between the high-pass filters b^1 and b^2. Indeed,

$$\begin{aligned} \widehat{b^2}(\xi) &= e^{-i\xi}\overline{\widehat{a^2}(\xi+\pi)} \approx e^{-i\xi}\overline{\widehat{a^1}(\xi+\pi)}e^{-i\theta(\xi+\pi)} \\ &= \widehat{b^1}(\xi)e^{i(\xi+\pi)/2}e^{-i\pi\lfloor\frac{\xi+2\pi}{2\pi}\rfloor} = -ie^{i\xi/2}\widehat{b^1}(\xi)e^{-i\pi\lfloor\frac{\xi}{2\pi}\rfloor}. \end{aligned} \tag{2.9}$$

Since $e^{-i\pi\lfloor\frac{\xi}{2\pi}\rfloor} = -1$ for $\xi \in [-\pi, 0)$ and $e^{-i\pi\lfloor\frac{\xi}{2\pi}\rfloor} = 1$ for $\xi \in [0, \pi)$, on the basic frequency interval $[-\pi, \pi)$, we have

$$\widehat{b^2}(\xi) \approx -i\,\mathrm{sgn}(\xi)e^{i\xi/2}\widehat{b^1}(\xi), \qquad \xi \in [-\pi, \pi). \tag{2.10}$$

In other words, the high-pass filters b^1 and b^2 are linked through a sort of the Hilbert transform in (2.10), which is similar to (1.4) and plays a critical role in producing directionality in high dimensions [24, 25, 33, 34].

The one-dimensional DT-$\mathbb{C}$WT employs two trees of the standard discrete orthogonal wavelet transform. The first tree uses the real-valued orthogonal wavelet filter bank $\{a^0; b^0\}$ for the first level and uses the real-valued orthogonal wavelet filter bank $\{a^1; b^1\}$ for the rest of the levels (that is, for the second and higher levels). The second tree uses the real-valued orthogonal wavelet filter bank $\{a^0(\cdot - 1); b^0(\cdot - 1)\}$ for the first level and uses the real-valued orthogonal wavelet filter bank $\{a^2; b^2\}$ for the rest of the levels. See Figure 3 for an illustration of the two-level DT-$\mathbb{C}$WT. Then the corresponding high-pass wavelet coefficients from these two trees are mixed together pairwise by forming complex coefficients through averages and differences. For an excellent detailed explanation of the DT-$\mathbb{C}$WT, see the tutorial article [34] and many references therein.

We now explain the one-dimensional DT-$\mathbb{C}$WT from the viewpoint of discrete affine systems. Since the first level of the DT-$\mathbb{C}$WT uses two orthogonal wavelet filter banks $\{a^0; b^0\}$ and $\{a^0(\cdot - 1); b^0(\cdot - 1)\}$, putting them together, we have a tight framelet filter bank $2^{-1/2}\{a^0, a^0(\cdot - 1); b^0, b^0(\cdot - 1)\}$, which is exactly the underlying tight framelet filter bank for the one-dimensional undecimated wavelet transform using the orthogonal wavelet filter bank $\{a^0; b^0\}$. After forming complex wavelet coefficients for high-pass coefficients by taking averages and differences, the first level of the DT-$\mathbb{C}$WT actually employs the complex-valued high-pass filters as follows:

$$b_1^p := [b^0 + ib^0(\cdot - 1)]/\sqrt{2} \quad \text{and} \quad b_1^n := [b^0 - ib^0(\cdot - 1)]/\sqrt{2}, \tag{2.11}$$

where the superscripts p and n refer to positive and negative in the frequency domain. It is trivial to directly check that $2^{-1/2}\{a^0, a^0(\cdot - 1); b_1^p, b_1^n\}$ is indeed a tight framelet filter bank. Define

$$a_1^1 := a^0, \quad a_1^2 := a^0(\cdot - 1). \tag{2.12}$$

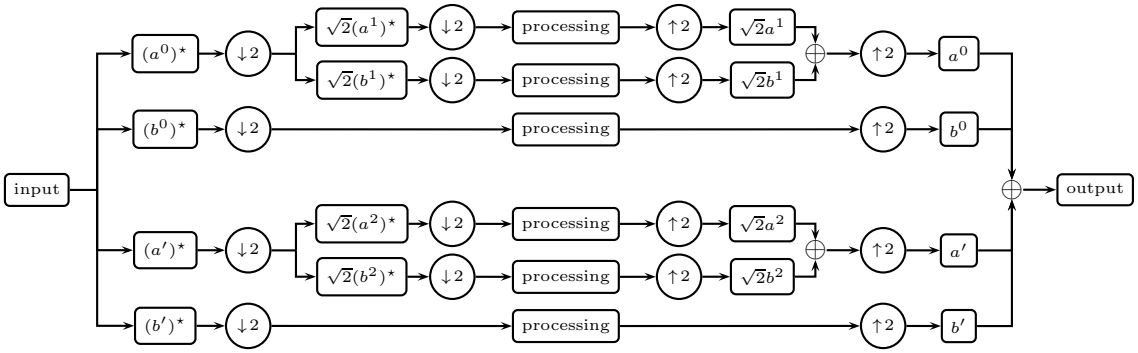

Figure 3. *Diagram of the one-dimensional two-level* DT-$\mathbb{C}$WT *(before forming complex wavelet coefficients) using an initial orthogonal wavelet filter bank* $\{a^0; b^0\}$ *and a pair of correlated orthogonal wavelet filter banks* $\{a^1; b^1\}$ *and* $\{a^2; b^2\}$. *Note that* $a' := a^0(\cdot - 1)$ *and* $b' := b^0(\cdot - 1)$. *The top is tree one and the bottom is tree two.*

The first level of the DT-$\mathbb{C}$WT in fact uses the tight framelet filter bank $2^{-1/2}\{a_1^1, a_1^2; b_1^p, b_1^n\}$, which has two real-valued low-pass filters a_1^1, a_1^2 and two complex-valued high-pass filters b_1^p, b_1^n. The one-level underlying discrete affine system is simply $\mathsf{DAS}_1(2^{-1/2}\{a_1^1, a_1^2; b_1^p, b_1^n\})$, more explicitly,

$$\mathsf{DAS}_1(a^0, a^1, a^2 \mid \text{DT-}\mathbb{C}\text{WT}) := \{a_1^1(\cdot - 2k), a_1^2(\cdot - 2k) \ : \ k \in \mathbb{Z}\} \cup \{b_1^p(\cdot - 2k), b_1^n(\cdot - 2k) \ : \ k \in \mathbb{Z}\}.$$

We now look at the DT-$\mathbb{C}$WT for higher levels $J \ge 2$. At level J, we use two real-valued orthogonal wavelet filter banks $\{a^1; b^1\}$ and $\{a^2; b^2\}$. The underlying J-level discrete affine system for $J \ge 2$ is

$$\begin{aligned}\mathsf{DAS}_J(a^0, a^1, a^2 \mid \text{DT-}\mathbb{C}\text{WT}) :=& \{a_J^1(\cdot - 2^J k), a_J^2(\cdot - 2^J k) \ : \ k \in \mathbb{Z}\} \cup \\ & \bigcup_{j=1}^{J} \{b_j^p(\cdot - 2^j k), b_j^n(\cdot - 2^j k) \ : \ k \in \mathbb{Z}\},\end{aligned}$$

where the multilevel filters $a_j^1, a_j^2, b_j^p, b_j^n$ for $j \ge 2$ are defined to be

$$\widehat{a_j^1}(\xi) := 2^{(j-1)/2}\widehat{a^0}(\xi)\widehat{a^1}(2\xi)\cdots\widehat{a^1}(2^{j-2}\xi)\widehat{a^1}(2^{j-1}\xi), \tag{2.13}$$

$$\widehat{a_j^2}(\xi) := 2^{(j-1)/2}\widehat{a^0(\cdot - 1)}(\xi)\widehat{a^2}(2\xi)\cdots\widehat{a^2}(2^{j-2}\xi)\widehat{a^2}(2^{j-1}\xi), \tag{2.14}$$

$$b_j^p := [b_j^1 + ib_j^2]/\sqrt{2}, \qquad b_j^n := [b_j^1 - ib_j^2]/\sqrt{2} \tag{2.15}$$

with

$$\widehat{b_j^1}(\xi) := \widehat{a_{j-1}^1}(\xi)\widehat{b^1}(2^{j-1}\xi), \quad \widehat{b_j^2}(\xi) := \widehat{a_{j-1}^2}(\xi)\widehat{b^2}(2^{j-1}\xi).$$

In other words,

$$\mathsf{DAS}_J(a^0, a^1, a^2 \mid \text{DT-}\mathbb{C}\text{WT}) = \{a_{J;k}^1, a_{J;k}^2 \ : \ k \in \mathbb{Z}\} \cup \cup_{j=1}^{J}\{b_{j;k}^p, b_{j;k}^n \ : \ k \in \mathbb{Z}\}, \tag{2.16}$$

where

$$a^1_{j;k} := a^1_j(\cdot - 2^j k), \quad a^2_{j;k} := a^2_j(\cdot - 2^j k), \quad b^p_{j;k} := b^p_j(\cdot - 2^j k), \quad b^n_{j;k} := b^n_j(\cdot - 2^j k), \quad k \in \mathbb{Z}, j \in \mathbb{N}.$$

Moreover, for every integer $J \in \mathbb{N}$, the J-level discrete affine system $\mathsf{DAS}_J(a^0, a^1, a^2 \mid \text{DT-}\mathbb{C}\text{WT})$ is a (normalized) tight frame for $l_2(\mathbb{Z})$, that is,

$$v = \sum_{k\in\mathbb{Z}} \Big(\langle v, a^1_{J;k}\rangle a^1_{J;k} + \langle v, a^2_{J;k}\rangle a^2_{J;k} \Big) + \sum_{j=1}^{J} \sum_{k\in\mathbb{Z}} \Big(\langle v, b^p_{j;k}\rangle b^p_{j;k} + \langle v, b^n_{j;k}\rangle b^n_{j;k} \Big) \qquad \forall\, v \in l_2(\mathbb{Z})$$

with the series converging unconditionally in $l_2(\mathbb{Z})$. We also have the following cascade structure, on which the fast algorithm of the DT-$\mathbb{C}$WT is based:

$$\begin{aligned} &\sum_{k\in\mathbb{Z}} \Big(\langle v, a^1_{j-1;k}\rangle a^1_{j-1;k} + \langle v, a^2_{j-1;k}\rangle a^2_{j-1;k} \Big) \\ &\qquad = \sum_{k\in\mathbb{Z}} \Big(\langle v, a^1_{j;k}\rangle a^1_{j;k} + \langle v, a^2_{j;k}\rangle a^2_{j;k} + \langle v, b^p_{j;k}\rangle b^p_{j;k} + \langle v, b^n_{j;k}\rangle b^n_{j;k} \Big) \end{aligned}$$

for all $j \in \mathbb{N}$ and $v \in l_2(\mathbb{Z})$.

2.3. Frequency separation property of the one-dimensional DT-$\mathbb{C}$WT. To understand the directionality of the DT-$\mathbb{C}$WT in high dimensions, it is important to investigate the frequency separation of all the high-pass filters b^p_j, b^n_j in a J-level discrete affine system $\mathsf{DAS}_J(a^0, a^1, a^2 \mid \text{DT-}\mathbb{C}\text{WT})$. For every orthogonal low-pass filter a satisfying $\widehat{a}(0) = 1$ and $\widehat{a}(\pi) = 0$, it follows from the identity $|\widehat{a}(\xi)|^2 + |\widehat{a}(\xi+\pi)|^2 = 1$ that $\widehat{a}$ largely concentrates on $[-\pi/2, \pi/2]$; in other words, we often have $|\widehat{a}(\xi)|^2 \approx \chi_{[-\pi/2,\pi/2]}(\xi)$ for $\xi \in [-\pi, \pi)$.

We first study the frequency separation of b^p_1 and b^n_1 at level one. Since $\widehat{b^n_1}(\xi) = \overline{\widehat{b^p_1}(-\xi)}$ (that is, $b^n_1 = \overline{b^p_1}$) by (2.11), it suffices for us to look at the filter b^p_1. Since $\widehat{b^p_1}(\xi) = \frac{\sqrt{2}}{2}(1 + ie^{-i\xi})\widehat{b^0}(\xi)$ and $\widehat{b^0}(\xi) = e^{-i\xi}\overline{\widehat{a^0}(\xi+\pi)}$, for $\xi \in [-\pi, \pi)$, noting $|1 + ie^{-i\xi}|^2 = 2 + 2\sin\xi$, we have

$$|\widehat{b^p_1}(\xi)|^2 = (1+\sin\xi)|\widehat{a^0}(\xi+\pi)|^2 \approx (1+\sin\xi)\chi_{[-\pi,-\pi/2]}(\xi) + (1+\sin\xi)\chi_{[\pi/2,\pi]}(\xi).$$

Note that

$$\begin{aligned} &0 \le \sqrt{1+\sin\xi} \le 1 \quad \text{(small) on } [-\pi, -\pi/2], \\ &1 \le \sqrt{1+\sin\xi} \le \sqrt{2} \quad \text{(large) on } [\pi/2, \pi]. \end{aligned} \tag{2.17}$$

Therefore, $\widehat{b^p_1}$ concentrates more or less on the positive interval $[\pi/2, \pi) \subseteq [0, \pi)$ while $\widehat{b^p_1}$ is relatively small on the negative interval $[-\pi, 0]$. Consequently, by $\widehat{b^n_1}(\xi) = \overline{\widehat{b^p_1}(-\xi)}$, $\widehat{b^n_1}$ concentrates more or less on the negative interval $[-\pi, 0]$ and $\widehat{b^n_1}$ is relatively small on the positive interval $[0, \pi)$.

As noticed in [34, page 136], the high-pass filters b^p_1, b^n_1 for the first level of the DT-$\mathbb{C}$WT do not have nearly ideal frequency separation. Ideally, we prefer that $\widehat{b^p_1}$ vanish on $[-\pi, 0]$

so that $\widehat{b_1^p}$ concentrates largely on the positive interval $[0,\pi]$, while we prefer that $\widehat{b_1^n}$ vanish on $[0,\pi]$ so that $\widehat{b_1^n}$ concentrates largely on the negative interval $[-\pi,0]$. Hence, a natural quantity to measure frequency separation of b_1^p and b_1^n is $|\widehat{b_1^p}(\xi+\pi)|^2+|\widehat{b_1^n}(\xi)|^2$ for $\xi\in[0,\pi]$ (the smaller the quantity, the better the frequency separation). However, we always have the following identities:

$$\begin{aligned}&|\widehat{b_1^p}(\xi+\pi)|^2+|\widehat{b_1^n}(\xi)|^2=1-\sin\xi,\quad \xi\in[-\pi,\pi],\quad \text{and}\\&\int_0^\pi\big[|\widehat{b_1^p}(\xi+\pi)|^2+|\widehat{b_1^n}(\xi)|^2\big]d\xi=\pi-2.\end{aligned}\tag{2.18}$$

Indeed, it is easy to directly check that

$$|\widehat{b_1^p}(\xi+\pi)|^2=(1-\sin\xi)|\widehat{a^0}(\xi)|^2,\qquad |\widehat{b_1^n}(\xi)|^2=(1-\sin\xi)|\widehat{a^0}(\xi+\pi)|^2.$$

Now the identity in (2.18) follows directly from the above identities and the fact that $|\widehat{a^0}(\xi)|^2+|\widehat{a^0}(\xi+\pi)|^2=1$. Therefore, (2.18) implies that it is impossible to achieve $|\widehat{b_1^p}(\xi+\pi)|^2+|\widehat{b_1^n}(\xi)|^2\approx 0$ for all $\xi\in[0,\pi]$, regardless of the choice of the initial real-valued orthogonal wavelet filter bank $\{a^0;b^0\}$.

We now study the frequency separation of b_j^p and b_j^n for $j\geq 2$. By the half-shift condition in (2.8) and the definition of a_j^1 and a_j^2 in (2.13) and (2.14), we have

$$\widehat{a_j^2}(2^{-j}\xi)\approx\widehat{a_j^1}(2^{-j}\xi)e^{-i2^{-j}\xi}e^{i\sum_{\ell=1}^{j-1}\theta(2^{-\ell}\xi)}.\tag{2.19}$$

Using the terminating binary representation of a real number ξ, we can prove the following identity:

$$\sum_{\ell=1}^{\infty}\lfloor 2^{-\ell}\xi+\tfrac{1}{2}\rfloor=\lfloor\xi\rfloor+\frac{1-\operatorname{sgn}(\xi)}{2}=\begin{cases}\lfloor\xi\rfloor & \text{if } \xi\geq 0,\\ \lfloor\xi\rfloor+1 & \text{if } \xi<0.\end{cases}\tag{2.20}$$

By the definition of θ in (2.8) and the above identity, we have

$$\begin{aligned}\sum_{\ell=1}^{\infty}\theta(2^{-\ell}\xi)-\theta(\xi+\pi)&=\sum_{\ell=1}^{\infty}\Big(-2^{-\ell-1}\xi+\pi\lfloor 2^{-\ell}\tfrac{\xi}{2\pi}+\tfrac{1}{2}\rfloor\Big)-\Big(-\tfrac{\xi+\pi}{2}+\pi\lfloor\tfrac{\xi+2\pi}{2\pi}\rfloor\Big)\\&=-\frac{\pi}{2}+\pi\Big(\sum_{\ell=1}^{\infty}\lfloor 2^{-\ell}\tfrac{\xi}{2\pi}+\tfrac{1}{2}\rfloor-\lfloor\tfrac{\xi}{2\pi}\rfloor\Big)=-\frac{\pi}{2}\operatorname{sgn}(\xi)=\begin{cases}-\frac{\pi}{2} & \text{if } \xi\geq 0,\\ \frac{\pi}{2} & \text{if } \xi<0.\end{cases}\end{aligned}$$

By the above identity and noting that $\sum_{\ell=j}^{\infty}\theta(2^{-\ell}\xi)=-2^{-j}\xi+\sum_{\ell=j}^{\infty}\pi\lfloor 2^{-\ell}\frac{\xi}{2\pi}+\frac{1}{2}\rfloor$, we deduce that

$$\sum_{\ell=1}^{j-1}\theta(2^{-\ell}\xi)=\sum_{\ell=1}^{\infty}\theta(2^{-\ell}\xi)-\sum_{\ell=j}^{\infty}\theta(2^{-\ell}\xi)=-\tfrac{\xi}{2}+2^{-j}\xi+\pi\Big(\tfrac{1-\operatorname{sgn}(\xi)}{2}+\lfloor\tfrac{\xi}{2\pi}\rfloor-\sum_{\ell=j}^{\infty}\lfloor 2^{-\ell}\tfrac{\xi}{2\pi}+\tfrac{1}{2}\rfloor\Big).$$

When $\xi \in [-2^j\pi, 2^j\pi)$, we have $2^{-\ell}\frac{\xi}{2\pi} + \frac{1}{2} \in [0,1)$ for all $\ell \ge j$. Hence, it follows from the above identity that

$$\sum_{\ell=1}^{j-1} \theta(2^{-\ell}\xi) = -\tfrac{\xi}{2} + 2^{-j}\xi + \pi\Big(\tfrac{1-\mathrm{sgn}(\xi)}{2} + \lfloor \tfrac{\xi}{2\pi} \rfloor\Big), \qquad \xi \in [-2^j\pi, 2^j\pi).$$

Therefore, we deduce from (2.19) and the above identity that

$$\widehat{a_j^2}(\xi) \approx e^{-i2^{j-1}\xi}\widehat{a_j^1}(\xi)\eta(2^j\xi) \qquad \forall\, \xi \in [-\pi,\pi), j \ge 2, \tag{2.21}$$

where

$$\eta(\xi) := e^{i\pi\left(\frac{1-\mathrm{sgn}(\xi)}{2} + \lfloor \frac{\xi}{2\pi} \rfloor\right)} = \mathrm{sgn}(\xi) e^{i\pi \lfloor \frac{\xi}{2\pi} \rfloor}.$$

We see that $\eta(\xi) = (-1)^k$ for all $|\xi| \in [2\pi k, 2\pi(k+1))$ and $k \in \mathbb{N} \cup \{0\}$. In particular, $\eta(\xi) = 1$ for all $\xi \in [-2\pi, 2\pi)$. Since $|\widehat{a_j^1}(\xi)|^2 \approx 2^{j-1}\chi_{2^{-j}[-\pi,\pi)}(\xi)$ for $\xi \in [-\pi,\pi)$ and $\eta(2^j\xi) = 1$ for all $\xi \in 2^{1-j}[-\pi,\pi)$, we deduce from (2.21) that $\widehat{a_j^2}(\xi) \approx e^{-i2^{j-1}\xi}\widehat{a_j^1}(\xi)$ for all $\xi \in [-\pi,\pi)$, that is, $a_j^2 \approx a_j^1(\cdot - 2^{j-1})$ for $j \ge 2$.

Note that on the basic frequency interval $[-\pi,\pi)$, $|\widehat{a_{j-1}^2}(\xi)|^2 \approx 2^{j-2}\chi_{2^{1-j}[-\pi,\pi]}(\xi)$. Also note that $\eta(2^{j-1}\xi) = 1$ for $\xi \in 2^{2-j}[-\pi,\pi)$. Now by (2.10) and (2.21), for $\xi \in [-\pi,\pi)$, we have

$$\widehat{b_j^2}(\xi) = \widehat{a_{j-1}^2}(\xi)\widehat{b^2}(2^{j-1}\xi) \approx e^{-i2^{j-1}\xi}\widehat{a_{j-1}^1}(\xi)\eta(2^{j-1}\xi)(-i)\,\mathrm{sgn}(\xi)e^{i2^{j-1}\xi}\widehat{b^1}(2^{j-1}\xi) = -i\,\mathrm{sgn}(\xi)\widehat{b_j^1}(\xi).$$

That is, b_j^1 and b_j^2 are linked to each other through the Hilbert transform. Consequently, we have

$$\widehat{b_j^p}(\xi) = [\widehat{b_j^1}(\xi) + i\widehat{b_j^2}(\xi)]/\sqrt{2} \approx \widehat{b_j^1}(\xi)[1 + \mathrm{sgn}(\xi)]/\sqrt{2} = \begin{cases} 0 & \text{if } \xi \in [-\pi, 0), \\ \sqrt{2}\widehat{b_j^1}(\xi) & \text{if } \xi \in [0,\pi). \end{cases} \tag{2.22}$$

By the relation $\widehat{b_j^n}(\xi) = \overline{\widehat{b_j^p}(-\xi)}$, we see that $\widehat{b_j^n}(\xi) \approx 0$ for $\xi \in [0,\pi)$ and $\widehat{b_j^n}(\xi) \approx \sqrt{2}\widehat{b_j^1}(\xi)$ for $\xi \in [-\pi, 0]$. Therefore, b_j^p and b_j^n have nearly ideal frequency separation when $j \ge 2$. More precisely, $\widehat{b_j^p}$ vanishes nearly on the negative interval $[-\pi, 0)$ and concentrates largely on the positive interval $[0,\pi)$, while $\widehat{b_j^n}$ vanishes nearly on the positive interval $[0,\pi)$ and concentrates largely on the negative interval $[-\pi, 0)$.

2.4. Discrete affine systems for the two-dimensional DT-ℂWT. Though algorithmically the two-dimensional DT-ℂWT can be implemented using the tensor product of the one-dimensional DT-ℂWT, due to the mixing and pairing of the corresponding high-pass wavelet coefficients to form complex wavelet coefficients after the tensor product wavelet transform, the resulting discrete affine systems for the two-dimensional DT-ℂWT are not the tensor product of discrete affine systems for the one-dimensional DT-ℂWT; more precisely, they are not obtained by $\{a_j^1, a_j^2; b_j^p, b_j^n\} \otimes \{a_j^1, a_j^2; b_j^p, b_j^n\}$. In fact, to achieve better directionality, there is a further frequency separation for the pair (a_j^1, a_j^2) of low-pass filters by using a similar

technique as in (2.15) for the high-pass filters b_j^1 and b_j^2. Let us explain the details in the following. Define

$$a_j^p := [a_j^1 + ia_j^2]/\sqrt{2}, \qquad a_j^n := [a_j^1 - ia_j^2]/\sqrt{2}, \qquad j \in \mathbb{N}. \tag{2.23}$$

Then it is trivial to see that $\{a_{J;k}^p, a_{J;k}^n \ : \ k \in \mathbb{Z}\} \cup \cup_{j=1}^J \{b_{j;k}^p, b_{j,k}^n \ : \ k \in \mathbb{Z}\}$ is still a tight frame for $l_2(\mathbb{Z})$ and the following identity holds:

$$\sum_{k\in\mathbb{Z}} \Big(\langle v, a_{J;k}^1\rangle a_{J;k}^1 + \langle v, a_{J;k}^2\rangle a_{J;k}^2\Big) = \sum_{k\in\mathbb{Z}} \Big(\langle v, a_{J;k}^p\rangle a_{J;k}^p + \langle v, a_{J;k}^n\rangle a_{J;k}^n\Big) \tag{2.24}$$
$$\forall\, v \in l_2(\mathbb{Z}), J \in \mathbb{N}.$$

In the J-level discrete affine system for the two-dimensional DT-$\mathbb{C}$WT, its low-pass part has four real-valued low-pass filters and is obtained from the low-pass part in the tensor product $\{a_J^1, a_J^2; b_J^p, b_J^n\} \otimes \{a_J^1, a_J^2; b_J^p, b_J^n\}$, that is,

$$\mathrm{LP}_J := \{a_J^1, a_J^2\} \otimes \{a_J^1, a_J^2\} = \{a_J^1 \otimes a_J^1, a_J^1 \otimes a_J^2, a_J^2 \otimes a_J^1, a_J^2 \otimes a_J^2\},$$

and its high-pass part has 12 complex-valued high-pass filters in total and is taken from the high-pass part in the tensor product $\{a_j^p, a_j^n; b_j^p, b_j^n\} \otimes \{a_j^p, a_j^n; b_j^p, b_j^n\}$, that is,

$$\mathrm{HP}_j := \{a_j^p \otimes b_j^p, a_j^p \otimes b_j^n, a_j^n \otimes b_j^p, a_j^n \otimes b_j^n, b_j^p \otimes a_j^p, b_j^p \otimes a_j^n, b_j^p \otimes b_j^p, b_j^p \otimes b_j^n, b_j^n \otimes a_j^p, b_j^n \otimes a_j^n, b_j^n \otimes b_j^p, b_j^n \otimes b_j^n\}.$$

Now the J-level discrete affine system for the two-dimensional DT-$\mathbb{C}$WT with complex-valued high-pass filters is

$$\begin{aligned}\mathsf{DAS}_J(a^0, a^1, a^2 \,|\, 2\mathbb{D} \ \text{DT-}\mathbb{C}\text{WT}) :=& \{u(\cdot - 2^J k) \ : \ u \in \mathrm{LP}_J, k \in \mathbb{Z}^2\} \cup \\ & \bigcup_{j=1}^J \{v(\cdot - 2^j k) \ : \ v \in \mathrm{HP}_j, k \in \mathbb{Z}^2\}.\end{aligned}$$

At the level one, on $[-\pi, \pi)$, we have

$$\widehat{a_1^p}(\xi) = [\widehat{a_1^1}(\xi) + i\widehat{a_1^2}(\xi)]/\sqrt{2} = \widehat{a^0}(\xi)(1 + ie^{-i\xi})/\sqrt{2} \quad \text{and} \quad |\widehat{a_1^p}(\xi)| = |\widehat{a^0}(\xi)|\sqrt{1 + \sin\xi}. \tag{2.25}$$

By (2.17), we see that $\widehat{a_1^p}$ concentrates more or less on the positive interval $[\pi/2, \pi) \subseteq [0, \pi)$ while $\widehat{a_1^p}$ is relatively small on the negative interval $[-\pi, 0]$. By $\widehat{a_1^n}(\xi) = \overline{\widehat{a_1^p}(-\xi)}$, we see that $\widehat{a_1^n}$ concentrates more or less on the negative interval $[\pi, 0]$ while $\widehat{a_1^n}$ is relatively small on the positive interval $[0, \pi)$.

By the relation in (2.21) for $j \geq 2$, we have

$$\widehat{a_j^p}(\xi) = [\widehat{a_j^1}(\xi) + i\widehat{a_j^2}(\xi)]/\sqrt{2} \approx \widehat{a_j^1}(\xi)(1 + ie^{-i2^{j-1}\xi})\eta(2^j\xi)/\sqrt{2}.$$

Since $|\widehat{a_j^1}(\xi)|^2 \approx 2^{j-1}\chi_{2^{-j}[-\pi,\pi)}(\xi)$ for $\xi \in [-\pi, \pi)$ and $\eta(2^j\xi) = 1$ for $\xi \in 2^{1-j}[-\pi, \pi)$, we conclude that

$$\begin{aligned}|\widehat{a_j^p}(\xi)| &= \sqrt{1 + \sin(2^{j-1}\xi)}|\widehat{a_j^1}(\xi)| \\ &\approx 2^{(j-1)/2}\sqrt{1 + \sin(2^{j-1}\xi)}\chi_{2^{-j}[-\pi,\pi)}(\xi), \qquad \xi \in [-\pi, \pi).\end{aligned} \tag{2.26}$$

Note that $0 \le \sqrt{1+\sin(2^{j-1}\xi)} \le 1$ (small) for $\xi \in 2^{-j}[-\pi, 0]$ and $1 \le \sqrt{1+\sin(2^{j-1}\xi)} \le \sqrt{2}$ (large) for $\xi \in 2^{-j}[0, \pi)$. Therefore, on the basic frequency interval $[-\pi, \pi)$, $\widehat{a_j^p}$ concentrates largely inside $[0, 2^{-j}\pi) \subseteq [0, \pi)$ and $\widehat{a_j^p}$ is relatively small on $[-\pi, 0)$, while $\widehat{a_j^n}$ concentrates largely inside $[-2^{-j}\pi, 0] \subseteq [-\pi, 0]$ and $\widehat{a_j^n}$ is relatively small on $[0, \pi)$.

For a sequence $u : \mathbb{Z}^d \to \mathbb{C}$, we can write $u = u^{[r]} + iu^{[i]}$ with both $u^{[r]}$ and $u^{[i]}$ being real-valued filters; that is, $u^{[r]}$ and $u^{[i]}$ are the real and imaginary parts of the filter u. As we will explain in subsection 6.2, though every complex-valued high-pass filter $u \in \mathsf{DAS}_J(a^0, a^1, a^2 \,|\, 2\mathbb{D}$ DT-$\mathbb{C}$WT$)$ does not have any directionality, its real part $u^{[r]}$ and imaginary part $u^{[i]}$ have directionality. In fact, the directional discrete affine system for the two-dimensional DT-$\mathbb{C}$WT is $\{u^{[r]}, u^{[i]} : u \in \mathsf{DAS}_J(a^0, a^1, a^2 \,|\, 2\mathbb{D}$ DT-$\mathbb{C}$WT$)\}$, the real-valued version, which is also a tight frame for $l_2(\mathbb{Z}^2)$. Due to the relation $\widehat{a_j^n}(\xi) = \overline{\widehat{a_j^p}(-\xi)}$ and $\widehat{b_j^n}(\xi) = \overline{\widehat{b_j^p}(-\xi)}$, we have $a_j^n = \overline{a_j^p}$ and $b_j^n = \overline{b_j^p}$. Hence, there are essentially 12 real-valued high-pass filters in HP_j having the following directions:

(1) the real and imaginary parts of $b_j^p \otimes a_j^p$ (or $b_j^n \otimes a_j^n$) have direction along 15°;
(2) the real and imaginary parts of $b_j^p \otimes a_j^n$ (or $b_j^n \otimes a_j^p$) have direction along −15°;
(3) the real and imaginary parts of $a_j^p \otimes b_j^p$ (or $a_j^n \otimes b_j^n$) have direction along 75°;
(4) the real and imaginary parts of $a_j^p \otimes b_j^n$ (or $a_j^n \otimes b_j^p$) have direction along −75°;
(5) the real and imaginary parts of $b_j^p \otimes b_j^p$ (or $b_j^n \otimes b_j^n$) have direction along 45°;
(6) the real and imaginary parts of $b_j^p \otimes b_j^n$ (or $b_j^n \otimes b_j^p$) have direction along −45°.

From the above discussion, we see that for level $j \ge 2$, the two-dimensional DT-$\mathbb{C}$WT has strong directions along ±45° due to the nearly ideal frequency separation in (2.22), while the directions along ±15° and ±75° are not that strong or ideal, due to the weak frequency separation in (2.26). For the initial level $j = 1$, the two-dimensional DT-$\mathbb{C}$WT has weak directions along all ±15°, ±45°, and ±75°.

3. The DT-$\mathbb{C}$WT using frequency-based filter banks. In this section, we shall look at various filter banks used in the DT-$\mathbb{C}$WT and then compare their performance for the problem of image denoising. On one hand, finitely supported filter banks are of importance and interest in many applications, due to their computational efficiency and good space/time localization. On the other hand, it is easy to design filter banks in the frequency domain to satisfy (1.1) and (1.2) for constructing tight framelet filter banks. Moreover, the frequency separation and frequency localization of the elements in discrete affine systems are two critical ingredients for the impressive performance of the discrete framelet/wavelet transform in many applications. For application of the DT-$\mathbb{C}$WT to image denoising, we shall see in this section that the DT-$\mathbb{C}$WT, employing a pair of frequency-based correlated orthogonal wavelet filter banks, performs equally well as the original DT-$\mathbb{C}$WT employing a pair of finitely supported correlated orthogonal wavelet filter banks proposed and commonly used in [24, 25, 34, 35, 36] and references therein.

We first recall the finitely supported orthogonal wavelet filter banks which have been commonly used in the DT-$\mathbb{C}$WT and have been designed by Kingsbury and Selesnick in [24, 34, 35, 36].

By $l_0(\mathbb{Z})$ we denote all finitely supported sequences on $\mathbb{Z}$. Since $e^{i\theta(\xi)}$ in (2.8) is not a 2π-periodic trigonometric polynomial, if both a^1 and a^2 are finitely supported filters from

$l_0(\mathbb{Z})$, then the half-shift condition in (2.8) can be only approximately satisfied. Many finitely supported pairs $\{a^1; b^1\}$ and $\{a^2; b^2\}$ approximately satisfying (2.8) have been constructed in [24, 25, 33, 34] and references therein. Here we list only one pair which has been implemented and frequently used for the purpose of image denoising by the research groups of Kingsbury and Selesnick. Such filters are posted at http://eeweb.poly.edu/iselesni/WaveletSoftware/. The initial filter a^0 is given by

$$\begin{aligned} a^0 &= \Big\{-\tfrac{1}{16}, \tfrac{1}{16}, \tfrac{4+\sqrt{15}}{16}, \tfrac{4+\sqrt{15}}{16}, \tfrac{1}{16}, -\tfrac{1}{16}, \tfrac{4-\sqrt{15}}{16}, \tfrac{4-\sqrt{15}}{16}\Big\}_{[-3,4]} \\ &\approx 2^{-1/2}\{-0.08838834764832, 0.08838834764832, 0.695879989034, \\ &\qquad 0.695879989034, 0.08838834764832, -0.08838834764832, \\ &\qquad 0.01122679215254, 0.01122679215254\}_{[-3,4]}. \end{aligned} \tag{3.1}$$

The correlated pair (a^1, a^2) of real-valued orthogonal filters has been constructed by Kingsbury [24] as follows:

$$\begin{aligned} a^1 = 2^{-1/2}\{&0.03516384, 0, -0.08832942, 0.23389032, 0.76027237, \\ &0.5875183, 0, -0.11430184\}_{[-4,3]}, \end{aligned} \tag{3.2}$$

$$\widehat{a^2}(\xi) := e^{-i\xi}\overline{\widehat{a^1}(\xi)}. \tag{3.3}$$

To analyze some properties of the orthogonal low-pass filters a^0 and a^1, we now recall some definitions and notation. For a finitely supported filter $a : \mathbb{Z} \to \mathbb{C}$, we define its sum rule order to be $\mathrm{sr}(a) := m$, where m is the largest nonnegative integer such that $\widehat{a}(\xi) = (1 + e^{-i\xi})^m \widehat{u}(\xi)$ for some 2π-periodic trigonometric polynomial $\widehat{u}$; in other words, $\widehat{a}(\xi + \pi) = \mathcal{O}(|\xi|^m)$ as $\xi \to 0$. The *smoothness exponent* of the low-pass filter a (see [5, 14]) is defined to be

$$\mathrm{sm}(a) := -1/2 - \log_2 \sqrt{\rho(u)}, \tag{3.4}$$

where $\rho(u)$ denotes the spectral radius—the largest of the modulus of all the eigenvalues—of the square matrix $(v(2j-k))_{-K\le j,k\le K}$, where v is determined by $\sum_{k=-K}^{K} v(k)e^{-ik\xi} := |\widehat{u}(\xi)|^2$. The larger the quantity $\mathrm{sm}(a)$, the smoother its associated refinable function ϕ^a, which is defined to be $\widehat{\phi^a}(\xi) := \prod_{j=1}^{\infty} \widehat{a}(2^{-j}\xi)$. For a finitely supported high-pass filter b, we define its vanishing moment order to be $\mathrm{vm}(b) := n$, where n is the largest integer such that $\widehat{b}(\xi) = (1 - e^{-i\xi})^n \widehat{v}(\xi)$ for some 2π-periodic trigonometric polynomial, that is, $\widehat{b}(\xi) = \mathcal{O}(|\xi|^n)$ as $\xi \to 0$.

The filter a^0 in (3.1) is a real-valued orthogonal low-pass filter with $\mathrm{sr}(a) = 2$ and $\mathrm{sm}(a^0) \approx 1.509402$. Hence, its associated high-pass filter b^0 has two vanishing moments by $\mathrm{vm}(b^0) = 2$. Note that a^0 is almost symmetric about the point $-1/2$. Therefore, $\widehat{a^0}(\xi) \approx |\widehat{a^0}(\xi)|e^{i\xi/2}$. The MATLAB program, which is posted on Selesnick's web page and implements the DT-$\mathbb{C}$WT, uses the filter bank $\{(a^0)^\star; (b^0)^\star\}$ instead of $\{a^0(\cdot - 1); b^0(\cdot - 1)\}$ for the first level in the second tree, where $(a^0)^\star$ is the adjoint filter of a^0 which is defined by $\widehat{(a^0)^\star}(\xi) := \overline{\widehat{a^0}(\xi)}$. This yields

the same effect as using $\{a^0(\cdot-1); b^0(\cdot-1)\}$ since we still have the one-shift condition as follows:

$$\widehat{(a^0)^\star}(\xi) = \overline{\widehat{a^0}(\xi)} \approx |\widehat{a^0}(\xi)|e^{-i\xi/2} = e^{-i\xi}|\widehat{a^0}(\xi)|e^{i\xi/2} \approx e^{-i\xi}\widehat{a^0}(\xi).$$

The filter a^1 in (3.2) is a real-valued orthogonal low-pass filter with $\mathrm{sr}(a^1) = 1$ and $\mathrm{sm}(a^1) \approx 0.997590$. Hence, the high-pass filters b^1 and b^2 have only one vanishing moment by $\mathrm{vm}(b^1) = \mathrm{vm}(b^2) = 1$. The filter a^1 is designed in such a way that it satisfies the quarter-shift condition

$$\widehat{a^1}(\xi) \approx |\widehat{a^1}(\xi)|e^{-i\xi/4}, \qquad \xi \in [-\pi, \pi), \tag{3.5}$$

so that we have the half-shift condition in (2.8) as follows:

$$\widehat{a^2}(\xi) = e^{-i\xi}\overline{\widehat{a^1}(\xi)} \approx e^{-i\xi}|\widehat{a^1}(\xi)|e^{i\xi/4} = e^{-i\xi/2}|\widehat{a^1}(\xi)|e^{-i\xi/4} \approx e^{-i\xi/2}\widehat{a^1}(\xi).$$

See Figure 4 for several graphs associated with the orthogonal filters a^0 and a^1.

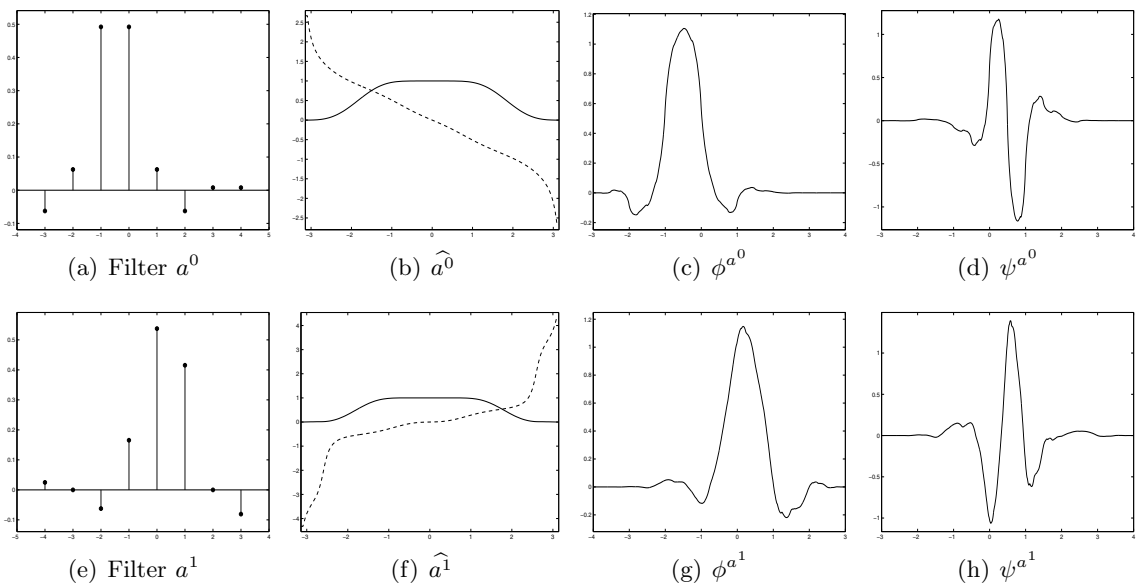

(a) Filter a^0 (b) $\widehat{a^0}$ (c) ϕ^{a^0} (d) ψ^{a^0}

(e) Filter a^1 (f) $\widehat{a^1}$ (g) ϕ^{a^1} (h) ψ^{a^1}

Figure 4. *Filters, magnitudes and phases, refinable functions, and wavelet functions associated with a^0 and a^1. The solid lines in* (b) *and* (f) *represent the magnitude, and the dotted lines in* (b) *and* (f) *refer to the phase of the filters in the frequency domain.*

As mentioned before, the half-shift condition in (2.8) can only be approximately satisfied if we restrict all filters to be finitely supported sequences from $l_0(\mathbb{Z})$. However, if we are allowed to use infinitely supported filters, then we indeed can easily satisfy the half-shift condition in (2.8) exactly. We now provide a pair of correlated orthogonal wavelet filter banks constructed in the frequency domain. Let $\mathsf{P}_m(x) := (1-x)^m \sum_{j=0}^{m-1} \binom{m+j-1}{j} x^j$. Then P_m satisfies the identity $\mathsf{P}_m(x) + \mathsf{P}_m(1-x) = 1$ (see [5]). For $c_L < c_R$ and two positive numbers $\varepsilon_L, \varepsilon_R$

satisfying $\varepsilon_L + \varepsilon_R \le c_R - c_L$, we now define a bump function $\chi_{[c_L,c_R];\varepsilon_L,\varepsilon_R}$ on $\mathbb{R}$ by

$$\chi_{[c_L,c_R];\varepsilon_L,\varepsilon_R}(\xi) := \begin{cases} 0, & \xi \le c_L - \varepsilon_L \text{ or } \xi \ge c_R + \varepsilon_R, \\ \sin\left(\frac{\pi}{2}\mathsf{P}_m(\frac{c_L+\varepsilon_L-\xi}{2\varepsilon_L})\right), & c_L - \varepsilon_L < \xi < c_L + \varepsilon_L, \\ 1, & c_L + \varepsilon_L \le \xi \le c_R - \varepsilon_R, \\ \sin\left(\frac{\pi}{2}\mathsf{P}_m(\frac{\xi-c_R+\varepsilon_R}{2\varepsilon_R})\right), & c_R - \varepsilon_R < \xi < c_R + \varepsilon_R. \end{cases} \tag{3.6}$$

Let $0 < \varepsilon \le \frac{\pi}{2}$. Define filters $a^0, a^1, a^2 \in l_1(\mathbb{Z})$ by

$$\widehat{a^0}(\xi) := \widehat{a^1}(\xi) := \chi_{[-\frac{\pi}{2},\frac{\pi}{2}];\varepsilon,\varepsilon}(\xi), \qquad \widehat{a^2}(\xi) := e^{-i\xi/2}\widehat{a^1}(\xi), \qquad \xi \in [-\pi,\pi). \tag{3.7}$$

Then all filters a^0, a^1, a^2 are real-valued orthogonal low-pass filters and the half-shift condition in (2.8) is satisfied exactly. If $\varepsilon = \frac{\pi}{6}$, then the filter a^0 is simply the Meyer orthogonal low-pass filter. Since all $\widehat{a^0}, \widehat{a^1}$, and $\widehat{a^2}$ belong to $C^{m-1}(\mathbb{T})$, the filters a^0, a^1, and a^2, despite having infinite support, have fast decaying coefficients. Using the discrete Fourier transform, the above frequency-based filter banks can be easily implemented with the same computational complexity as the discrete Fourier transform, that is, $\mathcal{O}(N \log N)$ with N inputs. The frequency-based implementation of the complex wavelet transform has been addressed in [4].

For simplicity of experiments on image denoising, we assume that the standard deviation σ_n of additive independent and identically distributed (i.i.d.) Gaussian noise is known in advance and all the numerical PSNR values are an average over five experiments. The five standard test images are from http://decsai.ugr.es/∼javier/denoise/test_images. All the PSNR values for the dual tree complex wavelet transform (DT-ℂWT) in this paper are obtained using the MATLAB program posted on Selesnick's web page at http://eeweb.poly.edu/iselesni/WaveletSoftware. This MATLAB program uses the finitely supported orthogonal filters a^0, a^1, a^2 in (3.1), (3.2), and (3.3), and we assume that the standard deviation σ_n is known in advance. Note that we use the standard definition $\text{PSNR} = 10\log_{10}\frac{255^2}{\text{MSE}}$ instead of $10\log_{10}\frac{256^2}{\text{MSE}}$ used in [35, 36], where MSE is the mean squared error.

As we shall see in Table 1 the performance on image denoising of the DT-ℂWT using the above frequency-based orthogonal filters a^0, a^1, a^2 in (3.7) with $\varepsilon = 189/256$ and $m = 1$ is comparable with the DT-ℂWT using the finitely supported orthogonal filters a^0, a^1, a^2 in (3.1), (3.2), and (3.3). Comparison results of the DT-ℂWT with other transform-based methods for image denoising have been well documented in [24, 35, 36].

4. Directional tensor product complex tight framelets. In this section we shall first construct one-dimensional complex tight framelet filter banks with good frequency separation property. Next we shall discuss their discrete affine systems and tensor product complex tight framelet filter banks in dimension two. Then we shall address application of such directional tensor product complex tight framelets for the problem of image denoising.

It has been observed in [19, section 7] that complex tight framelets can achieve better directionality than real-valued tight framelets. In particular, [19, section 7] provides an example of tensor product complex tight framelets exhibiting four directions in dimension two. Motivated by the example of complex tight framelets in [19], in this section we shall fully and

Table 1

Columns of $\mathbb{C}$WT *are for PSNR values (an average over five experiments) using bivariate shrinkage in* [36] *and the* DT-$\mathbb{C}$WT *using finitely supported orthogonal wavelet filter banks in* (3.1)–(3.3). *Columns of* F$\mathbb{C}$WT *are for PSNR values using the same bivariate shrinkage and the* DT-$\mathbb{C}$WT *using the frequency-based orthogonal wavelet filter banks in* (3.7).

	Lena		Barbara		Boat		House		Pepper	
σ_n	$\mathbb{C}$WT	F$\mathbb{C}$WT	$\mathbb{C}$WT	F$\mathbb{C}$WT	$\mathbb{C}$WT	F$\mathbb{C}$WT	$\mathbb{C}$WT	F$\mathbb{C}$WT	$\mathbb{C}$WT	F$\mathbb{C}$WT
5	38.25	38.25	37.36	37.44	36.77	36.77	38.45	38.41	37.18	37.13
10	35.19	35.20	33.52	33.60	33.21	33.19	34.78	34.73	33.40	33.31
15	33.47	33.46	31.38	31.45	31.33	31.29	32.90	32.85	31.29	31.19
20	32.23	32.22	29.87	29.94	30.01	29.96	31.63	31.58	29.83	29.71
25	31.26	31.24	28.70	28.78	28.99	28.95	30.65	30.59	28.71	28.57
30	30.47	30.44	27.77	27.84	28.18	28.14	29.84	29.78	27.80	27.66
50	28.21	28.18	25.26	25.31	26.01	25.98	27.57	27.52	25.30	25.18

further develop the idea in [19] by providing a systematic study and construction of directional tensor product complex tight framelets using discrete affine systems.

4.1. Tensor product complex tight framelets TP-$\mathbb{C}$TF$_{2s+1}$ with $s \in \mathbb{N}$. We now construct one-dimensional complex tight framelet filter banks whose tensor products lead to directional complex tight framelets in high dimensions. Before constructing such one-dimensional complex tight framelet filter banks, we first provide a road map and some explanation for our construction. In the following, we are interested in constructing one-dimensional complex tight framelet filter banks $\{a; b^{1,p}, \dots, b^{s,p}, b^{1,n}, \dots, b^{s,n}\}$ such that the following hold:

(1) $\{a; b^{1,p}, \dots, b^{s,p}, b^{1,n}, \dots, b^{s,n}\}$ is a tight framelet filter bank; that is, the following conditions are satisfied:

$$|\widehat{a}(\xi)|^2 + \sum_{\ell=1}^{s} |\widehat{b^{\ell,p}}(\xi)|^2 + \sum_{m=1}^{s} |\widehat{b^{m,n}}(\xi)|^2 = 1 \qquad \text{a.e. } \xi \in [-\pi, \pi], \tag{4.1}$$

$$\widehat{a}(\xi)\overline{\widehat{a}(\xi+\pi)} + \sum_{\ell=1}^{s} \widehat{b^{\ell,p}}(\xi)\overline{\widehat{b^{\ell,p}}(\xi+\pi)} + \sum_{m=1}^{s} \widehat{b^{m,n}}(\xi)\overline{\widehat{b^{m,n}}(\xi+\pi)} = 0 \tag{4.2}$$

$$\text{a.e. } \xi \in [-\pi, \pi].$$

(2) The low-pass filter a is real-valued, is symmetric about the origin, and has linear-phase moments of order $2m$ with phase zero: $\widehat{a}(\xi) = 1 + \mathcal{O}(|\xi|^{2m})$ as $\xi \to 0$ for some positive integer m. Roughly speaking, linear-phase moments of a low-pass filter mean that the associated refinable function with the low-pass filter has some polynomial preservation property; see [14, 17] for details. Linear-phase property (i.e., symmetry) and linear-phase moments of low-pass filters are desired, for example, in numerical algorithms and in applications in which information at different scales is considered together.

(3) All $\widehat{b^{1,p}}, \dots, \widehat{b^{s,p}}$ almost vanish on $[-\pi, 0]$ and concentrate on $[0, \pi]$.

(4) $b^{\ell,n} = \overline{b^{\ell,p}}$, that is, $\widehat{b^{\ell,n}}(\xi) = \overline{\widehat{b^{\ell,p}}(-\xi)}$ for all $\ell = 1, \dots, s$.

Except the condition $\widehat{a}(0) = 1$, the requirements in item (2) are not necessary for directionality but are desirable in applications. The linear-phase moments in item (2) imply that

$\widehat{a}(0)=1$ and all the high-pass filters $b^{\ell,p}, b^{\ell,n}$ have vanishing moments of order at least m (see [17]). The condition $\widehat{a}(0)=1$ is needed to guarantee the existence of a refinable function ϕ through $\widehat{\phi}(\xi):=\prod_{j=1}^{\infty}\widehat{a}(2^{-j}\xi)$. Item (3) is simply the frequency separation property. Item (4) allows us to reduce the redundancy of the associated underlying high-dimensional real-valued tight framelets which are obtained by separating the real and imaginary parts of the tensor product complex tight framelets in high dimensions. For simplicity, we further impose the following additional condition:

(5) $\widehat{a}(\xi)\widehat{a}(\xi+\pi)=0$ and $\widehat{b^{\ell,p}}(\xi)\widehat{b^{\ell,p}}(\xi+\pi)=0$ for all $\xi\in\mathbb{R}$ and $\ell=1,\ldots,s$.

The above conditions in item (5) directly imply (4.2). We now use the bump functions in (3.6) to construct one-dimensional complex tight framelet filter banks satisfying items (1)–(5) with all the constructed filters having fast decaying coefficients.

Let $0<c_1<c_2<\cdots<c_s<c_{s+1}:=\pi$. Let $\varepsilon_1,\ldots,\varepsilon_s$ be positive numbers satisfying

$$0<\varepsilon_1\le\min(c_1,\tfrac{\pi}{2}-c_1)\quad\text{and}\quad(c_{\ell+1}-c_\ell)+\varepsilon_{\ell+1}+\varepsilon_\ell\le\pi\qquad\forall\,\ell=1,\ldots,s. \tag{4.3}$$

Define a real-valued symmetric low-pass filter a by

$$\widehat{a}:=\chi_{[-c_1,c_1];\varepsilon_1,\varepsilon_1}, \tag{4.4}$$

and define $2s$ number of complex-valued high-pass filters $b^{1,p},\ldots,b^{s,p},b^{1,n},\ldots,b^{s,n}$ by

$$\widehat{b^{\ell,p}}:=\chi_{[c_\ell,c_{\ell+1}];\varepsilon_\ell,\varepsilon_{\ell+1}},\qquad\widehat{b^{\ell,n}}:=\overline{\widehat{b^{\ell,p}}(-\cdot)},\qquad\ell=1,\ldots,s. \tag{4.5}$$

The conditions in (4.3) guarantee item (5). It is easy to check that items (2)–(4) are satisfied with $m=\infty$ in item (2). Due to the definition of the bump functions in (3.6), we can also easily verify that the condition in (4.1) is satisfied. Therefore, $\mathbb{C}\mathrm{TF}_{2s+1}:=\{a;b^{1,p},\ldots,b^{s,p},b^{1,n},\ldots,b^{s,n}\}$ is a one-dimensional tight framelet filter bank satisfying all the conditions in items (1)–(5) such that all the high-pass filters have infinitely many vanishing moments. For simplicity, we often choose c_1 and ε_1 as free parameters and take

$$c_\ell:=c_1+\tfrac{\pi-c_1}{s}(\ell-1),\qquad\varepsilon_\ell=\varepsilon_1,\qquad\ell=1,\ldots,s. \tag{4.6}$$

For the particular choice in (4.6), due to the constraints in (4.3), the positive parameters c_1 and ε_1 must satisfy

$$0<\varepsilon_1\le\min(c_1,\tfrac{\pi}{2}-c_1,\tfrac{c_1+(s-1)\pi}{2s}). \tag{4.7}$$

The J-level discrete affine system for dimension one is simply $\mathsf{DAS}_J(\{a;b^{1,p},\ldots,b^{s,p},b^{1,n},\ldots,b^{s,n}\})$, which is defined at the beginning of section 2. The tensor product complex tight framelet filter bank TP-$\mathbb{C}\mathrm{TF}_{2s+1}$ for dimension two is simply

$$\begin{aligned}\text{TP-}\mathbb{C}\mathrm{TF}_{2s+1}&:=\mathbb{C}\mathrm{TF}_{2s+1}\otimes\mathbb{C}\mathrm{TF}_{2s+1}\\&=\{a;b^{1,p},\ldots,b^{s,p},b^{1,n},\ldots,b^{s,n}\}\otimes\{a;b^{1,p},\ldots,b^{s,p},b^{1,n},\ldots,b^{s,n}\}\end{aligned}$$

with $a\otimes a$ being the only low-pass filter and all other $4s(s+1)$ filters being high-pass filters. The J-level discrete affine system for dimension two is simply

$$\mathsf{DAS}_J(\text{TP-}\mathbb{C}\mathrm{TF}_{2s+1})=\mathsf{DAS}_J(\{a;b^{1,p},\ldots,b^{s,p},b^{1,n},\ldots,b^{s,n}\}\otimes\{a;b^{1,p},\ldots,b^{s,p},b^{1,n},\ldots,b^{s,n}\}).$$

TP-$\mathbb{C}$TF$_{2s+1}$ for dimension d can be defined similarly by taking d times the tensor product of $\mathbb{C}$TF$_{2s+1}$. For simplicity, we also use TP-$\mathbb{C}$TF$_{2s+1}$ to stand for $\mathbb{C}$TF$_{2s+1}$ for dimension one. Since TP-$\mathbb{C}$TF$_{2s+1}$ is a tensor product filter bank, as we discussed at the beginning of section 2, the discrete framelet transform using TP-$\mathbb{C}$TF$_{2s+1}$ is essentially the same as the classical tensor product discrete wavelet transform, except that we have more high-pass filters here than in the classical discrete orthogonal wavelet transform. The one-dimensional discrete framelet transform using TP-$\mathbb{C}$TF$_{2s+1}$ is illustrated in Figure 1 with the high-pass filters $b_1, \dots, b_s$ being replaced by $b^{1,p}, \dots, b^{s,p}, b^{1,n}, \dots, b^{s,n}$.

Note that the real and the imaginary parts of every complex-valued filter in TP-$\mathbb{C}$TF$_{2s+1}$ have the same directionality (see subsection 6.2). Due to the relations $b^{\ell,n} = \overline{b^{\ell,p}}$ for $\ell = 1, \dots, s$, we see that the $4s(s+1)$ high-pass filters in TP-$\mathbb{C}$TF$_{2s+1}$ exhibit $2s(s+1)$ different directions with the directions along $0°, 90°, \pm 45°$ degrees repeated $s-1$ times. Therefore, the tensor product complex tight framelet TP-$\mathbb{C}$TF$_{2s+1}$ for dimension two offers $2s(s+1) - 4(s-1) = 2s(s-1) + 4 = \frac{1}{2}(n-1)(n-3) + 4$ directions with $n := 2s+1$. For example, TP-$\mathbb{C}$TF$_3$ has four directions along $0°, \pm 45°$, and $90°$; TP-$\mathbb{C}$TF$_5$ has eight directions along $0°, \pm 22.5°, \pm 45°, \pm 67.5°$, and $90°$. The particular example constructed in [19] corresponds to TP-$\mathbb{C}$TF$_3$ here.

4.2. Tensor product complex tight framelets TP-$\mathbb{C}$TF$_{2s+2}$ with $s \in \mathbb{N}$. We now discuss how to further improve the directionality of TP-$\mathbb{C}$TF$_{2s+1}$ by splitting the low-pass filter a in $\mathbb{C}$TF$_{2s+1}$ into two auxiliary low-pass filters a^p and a^n. That is, the one-dimensional complex tight framelet filter bank is the same as TP-$\mathbb{C}$TF$_{2s+1}$, except that we further split the low-pass filter a into two low-pass filters a^p, a^n in the frequency domain. Let $0 < c_1 < c_2 < \cdots < c_s < c_{s+1} := \pi$, and let $\varepsilon_0, \varepsilon_1, \dots, \varepsilon_s$ be positive numbers satisfying (4.3) with the additional condition

$$0 < \varepsilon_0 < c_1 - \varepsilon_1. \tag{4.8}$$

Define a low-pass filter a and two auxiliary low-pass filters a^p, a^n by

$$\widehat{a} := \chi_{[-c_1,c_1];\varepsilon_1,\varepsilon_1}, \qquad \widehat{a^p} := \chi_{[0,c_1];\varepsilon_0,\varepsilon_1}, \qquad \widehat{a^n} := \overline{\widehat{a^p}(-\cdot)}. \tag{4.9}$$

The high-pass filters $b^{1,p}, \dots, b^{s,p}, b^{1,n}, \dots, b^{s,n}$ are defined as in (4.5). Note that $a^n = \overline{a^p}$. Since

$$|\widehat{a}(\xi)|^2 = |\widehat{a^p}(\xi)|^2 + |\widehat{a^n}(\xi)|^2 \quad \text{and} \quad \widehat{a}(\xi)\overline{\widehat{a}(\xi+\pi)} = \widehat{a^p}(\xi)\overline{\widehat{a^p}(\xi+\pi)} + \widehat{a^n}(\xi)\overline{\widehat{a^n}(\xi+\pi)}, \tag{4.10}$$

we can check that both $\mathbb{C}\text{TF}_{2s+1} = \{a; b^{1,p}, \dots, b^{s,p}, b^{1,n}, \dots, b^{s,n}\}$ and

$$\mathbb{C}\text{TF}_{2s+2} := \{a^p, a^n; b^{1,p}, \dots, b^{s,p}, b^{1,n}, \dots, b^{s,n}\}$$

are one-dimensional tight framelet filter banks. Note that the low-pass filter a is real-valued, is symmetric about the origin, and has infinitely many linear-phase moments. However, the auxiliary low-pass filters a^p and a^n are complex-valued and may not have any symmetry, but they satisfy the relation $a^n = \overline{a^p}$ and are one-sided in the frequency domain. In other words, the symmetric real-valued low-pass filter a is split into two complex-valued auxiliary low-pass

filters a^p and a^n satisfying $a^n = \overline{a^p}$ and (4.10). For simplicity, we often choose c_1, ε_0, and ε_1 as free parameters and take the special choice in (4.6). For this particular case, both (4.7) and (4.8) must be satisfied. We point out that one-sided low-pass filters have been employed in nonredundant complex Hilbert wavelet transforms in [39, 40]. As we shall see later, we use the technique of splitting a low-pass filter into two one-sided low-pass filters in order to improve directionality for high-dimensional tensor product complex tight framelets.

The J-level discrete affine system for dimension one is simply $\mathsf{DAS}_J(\{a; b^{1,p}, \ldots, b^{s,p}, b^{1,n}, \ldots, b^{s,n}\})$, which is defined at the beginning of section 2. However, the tensor product complex tight framelet filter bank for dimension two is a little bit more complicated by defining the high-pass parts TP-$\mathbb{C}$TF-HP$_{2s+2}$ through deleting all the low-pass parts $\{a^p, a^n\} \otimes \{a^p, a^n\}$ from the tensor product filter bank

$$\{a^p, a^n; b^{1,p}, \ldots, b^{s,p}, b^{1,n}, \ldots, b^{s,n}\} \otimes \{a^p, a^n; b^{1,p}, \ldots, b^{s,p}, b^{1,n}, \ldots, b^{s,n}\}. \tag{4.11}$$

More explicitly, TP-$\mathbb{C}$TF-HP$_{2s+2}$ consists of total $4s(s+2)$ high-pass filters:

$$a^p \otimes b^{\ell,p}, a^p \otimes b^{\ell,n}, a^n \otimes b^{\ell,p}, a^n \otimes b^{\ell,n}, b^{\ell,p} \otimes b^{m,p}, b^{\ell,p} \otimes b^{m,n}, b^{\ell,n} \otimes b^{m,p}, b^{\ell,n} \otimes b^{m,n}, \quad \ell, m = 1, \ldots, s.$$

Now it is not difficult to see that the tensor product complex tight framelet filter bank and the J-level discrete affine system for dimension two are given by

$$\text{TP-}\mathbb{C}\text{TF}_{2s+2} := \{a \otimes a; \text{TP-}\mathbb{C}\text{TF-HP}_{2s+2}\} \qquad \text{and} \qquad \mathsf{DAS}_J(\text{TP-}\mathbb{C}\text{TF}_{2s+2})$$

with $a \otimes a$ being the only low-pass filter in the two-dimensional tight framelet filter bank TP-$\mathbb{C}$TF$_{2s+2}$. TP-$\mathbb{C}$TF$_{2s+2}$ for dimension d can be defined similarly. For simplicity, we also use TP-$\mathbb{C}$TF$_{2s+2}$ to stand for $\mathbb{C}$TF$_{2s+2}$ for dimension one. Since TP-$\mathbb{C}$TF$_{2s+2}$ is almost a tensor product filter bank, the discrete framelet transform using TP-$\mathbb{C}$TF$_{2s+2}$ is essentially the tensor product discrete wavelet transform with a slight modification as follows:

(1) The tensor product filter bank in (4.11) is first applied to a two-dimensional input data v.

(2) The outputs from the four low-pass filters $a^p \otimes a^p, a^p \otimes a^n, a^n \otimes a^p, a^n \otimes a^n$ are discarded. Using the notation in section 2, these outputs are simply $2^{-1}\mathcal{T}_{a^p \otimes a^p} v$, $2^{-1}\mathcal{T}_{a^p \otimes a^n} v$, $2^{-1}\mathcal{T}_{a^n \otimes a^p} v$, $2^{-1}\mathcal{T}_{a^n \otimes a^n} v$.

(3) The tensor product low-pass filter $a \otimes a$ is applied to the input data v. The resulting output (that is, $2^{-1}\mathcal{T}_{a \otimes a} v$) is used as the single low-pass output to replace the four discarded outputs in item (2).

(4) Steps (1)–(3) are repeated recursively by treating the output from item (3) as the new input data.

In other words, the discrete framelet transform using TP-$\mathbb{C}$TF$_{2s+2}$ is essentially the same as the tensor product discrete framelet transform using the one-dimensional filter bank $\{a^p, a^n; b^{1,p}, \ldots, b^{s,p}, b^{1,n}, \ldots, b^{s,n}\}$ with the only modification that the outputs from the four auxiliary low-pass filters in $\{a^p, a^n\} \otimes \{a^p, a^n\}$ are replaced by the output from the single low-pass filter $a \otimes a$.

Due to $a^n = \overline{a^p}$ and $b^{\ell,n} = \overline{b^{\ell,p}}$ for $\ell = 1, \ldots, s$, we see that the $4s(s+2)$ high-pass filters in TP-$\mathbb{C}$TF-HP$_{2s+2}$ exhibit $2s(s+2)$ different directions with the directions along $\pm 45^\circ$ degrees

repeated $s-1$ times. Therefore, the tensor product complex tight framelet TP-$\mathbb{C}$TF$_{2s+2}$ for dimension two offers $2s(s+2)-2(s-1)=2(s-1)(s+2)+6=\frac{1}{2}(n-4)(n+2)+6$ directions with $n:=2s+2$. For example, TP-$\mathbb{C}$TF$_4$ has six directions along $\pm 15^\circ, \pm 45^\circ$, and $\pm 75^\circ$, and TP-$\mathbb{C}$TF$_6$ has 14 directions.

Throughout the paper, TP-$\mathbb{C}$TF$_3$ uses (4.6) with $c_1=\frac{33}{32}$ and $\varepsilon_1=\frac{69}{128}$, while TP-$\mathbb{C}TF_4$ uses (4.6) with $c_1=\frac{291}{128}$, $\varepsilon_0=\frac{35}{128}$, and $\varepsilon_1=\frac{27}{64}$; TP-$\mathbb{C}TF_6$ uses (4.6) with $c_1=\frac{119}{128}$, $\varepsilon_0=\frac{35}{128}$, and $\varepsilon_1=\frac{81}{128}$. See Figure 5 for graphs of the one-dimensional complex tight framelet filter banks $\mathbb{C}$TF$_3$, $\mathbb{C}$TF$_4$, and $\mathbb{C}$TF$_6$ in the frequency domain. See Figure 6 for the directionality of the two-dimensional tensor product complex tight framelet TP-$\mathbb{C}$TF$_3$ (more precisely, the generators in DAS_J(TP-$\mathbb{C}$TF$_3$)), Figure 7 for the directionality of the two-dimensional TP-$\mathbb{C}$TF$_4$, and Figure 8 for the directionality of the two-dimensional TP-$\mathbb{C}$TF$_6$. Except that TP-$\mathbb{C}$TF$_3$ has appeared in [19], all other TP-$\mathbb{C}$TF$_n$ with $n>3$ are new.

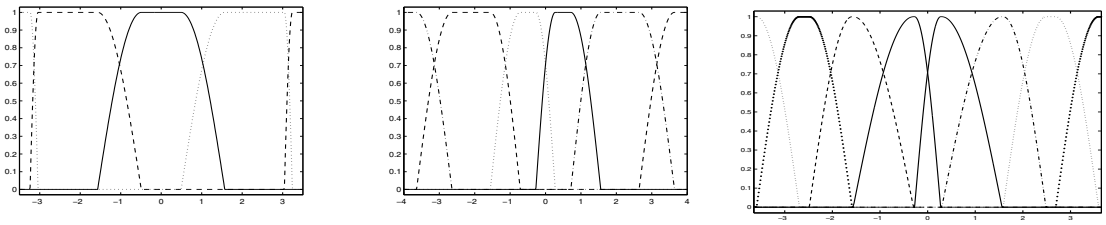

(a) $\mathbb{C}$TF$_3$ (b) $\mathbb{C}$TF$_4$ (c) $\mathbb{C}$TF$_6$

Figure 5. (a) *One-dimensional* $\mathbb{C}\mathrm{TF}_3=\{a;b^{1,p},b^{1,n}\}$ *in the frequency domain. Solid line is for low-pass filter* $\widehat{a}$. *Dotted line is for the high-pass filter* $\widehat{b^{1,p}}$. *Dashed line is for the high-pass filter* $\widehat{b^{1,n}}$. (b) *One-dimensional* $\mathbb{C}\mathrm{TF}_4=\{a^p,a^n;b^{1,p},b^{1,n}\}$ *in the frequency domain. Solid line is for the low-pass filter* $\widehat{a^p}$. *Dotted line is for the low-pass filter* $\widehat{a^n}$. *Dotted-dashed line is for the high-pass filter* $\widehat{b^{1,p}}$. *Dashed line is for the high-pass filter* $\widehat{b^{1,n}}$. (c) *One-dimensional* $\mathbb{C}\mathrm{TF}_6=\{a^p,a^n;b^{1,p},b^{2,p},b^{1,n},b^{2,n}\}$ *in the frequency domain. Right solid line is for* $\widehat{a^p}$ *and left solid line is for* $\widehat{a^n}$. *Dotted-dashed line is for* $\widehat{b^{1,p}}$ *and dotted line is for* $\widehat{b^{2,p}}$. *Dashed line is for* $\widehat{b^{1,n}}$ *and the line with* $+$ *sign is for* $\widehat{b^{2,n}}$.

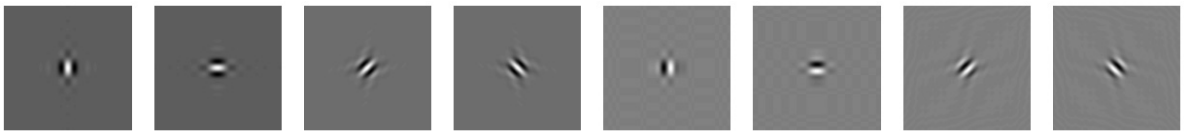

Figure 6. *The real part (the first four) and the imaginary part (the last four) of the generators at level* 5 *in* DAS_6(TP-$\mathbb{C}$TF$_3$).

4.3. Image denoising by tensor product complex tight framelets. Now we provide numerical experiments on image denoising using TP-$\mathbb{C}$TF$_n$ with $n\geq 3$. In all the experiments, bivariate shrinkage proposed in [35, 36] is applied to framelet coefficients. As shown in Tables 2–6, we can see clearly the improved performance in terms of PSNR due to improved directionality. The performance of TP-$\mathbb{C}$TF$_4$ is also comparable with that of the standard DT-$\mathbb{C}$WT using the finitely supported orthogonal wavelet filters in (3.1)–(3.3). In addition, the denoising results can be further improved by applying more complicated shrinkages such

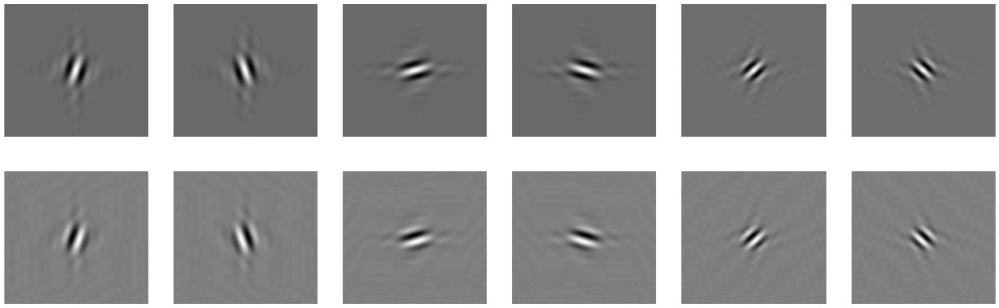

Figure 7. *The first row shows the real part and the second row shows the imaginary part of the generators at level* 5 *in* $\mathsf{DAS}_6(\text{TP-}\mathbb{C}\text{TF}_4)$.

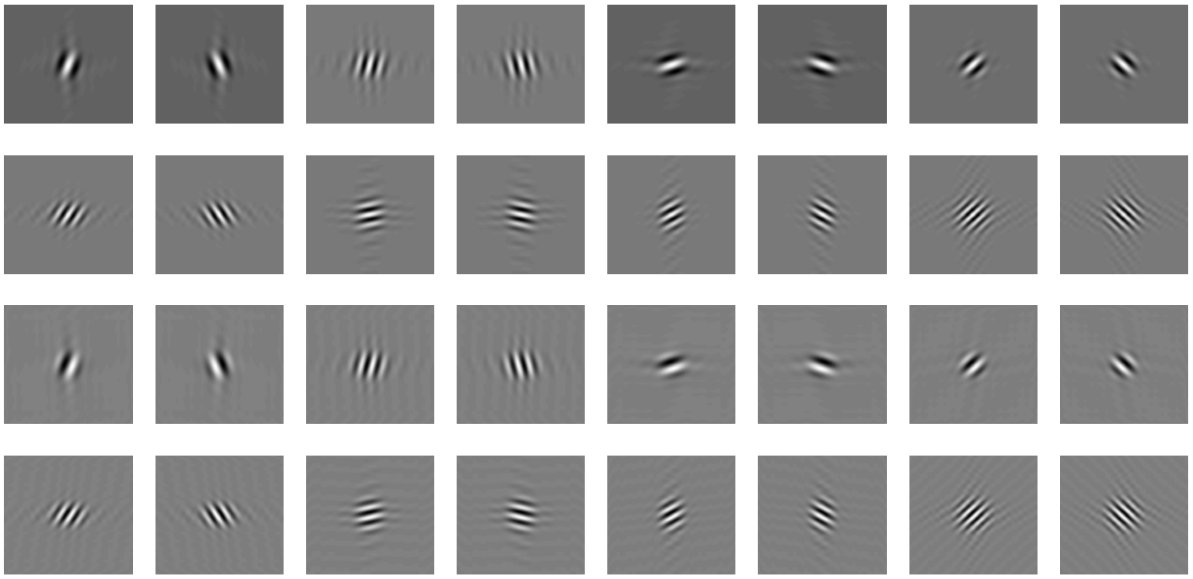

Figure 8. *The first two rows show the real part and the last two rows show the imaginary part of the generators at level* 5 *in* $\mathsf{DAS}_6(\text{TP-}\mathbb{C}\text{TF}_6)$. *Among these* 16 *graphs, the directions along* $\pm 45^\circ$ *are repeated once. Hence, there are a total of* 14 *directions in the discrete affine system* $\mathsf{DAS}_J(\text{TP-}\mathbb{C}\text{TF}_6)$.

as the Gaussian scale mixture model in [30] to the real and imaginary parts of the undecimated TP-$\mathbb{C}$TF$_n$ coefficients. As shown in Figures 9 and 10 for the test images of Lena and Barbara, due to improved directionality of tensor product complex tight framelets, the denoised images using TP-$\mathbb{C}$TF$_6$ not only have higher PSNR values but also have better visual quality than those using DT-$\mathbb{C}$WT.

5. Initial filter banks of the DT-$\mathbb{C}$WT. In this section we shall discuss the choice of the initial filter banks for the level one of the DT-$\mathbb{C}$WT. We shall see that tensor product complex tight framelets TP-$\mathbb{C}$TF$_n$ can be used as the initial filter banks in the DT-$\mathbb{C}$WT to further improve the directionality of the first level of the DT-$\mathbb{C}$WT. Performance of the DT-$\mathbb{C}$WT using TP-$\mathbb{C}$TF$_n$ as the initial filter bank for image denoising will be provided in this section.

The original DT-$\mathbb{C}$WT proposed by Kingsbury [24, 25] uses the initial filter banks $\{a^1; b^1\}$

Table 2

Denoising results for 512×512 *Lena image. Each numerical PSNR value is an average over five experiments.* σ_n *is the standard deviation of additive i.i.d. Gaussian noise and is assumed to be known in advance. Column* DT-$\mathbb{C}$WT *uses the* DT-$\mathbb{C}$WT *with a pair of correlated finitely supported orthogonal wavelet filter banks in* [24, 34] *(see* (3.1)–(3.3)*). Column* TP-$\mathbb{C}$TF$_3$ *uses tensor product complex tight framelet* TP-$\mathbb{C}$TF$_3$*. Columns* TP-$\mathbb{C}$TF$_4$ *and* $\mathbb{C}$TF$_4$*-GSM use tensor product complex tight framelet* TP-$\mathbb{C}$TF$_4$*. Columns* TP-$\mathbb{C}$TF$_6$ *and* $\mathbb{C}$TF$_6$*-GSM use tensor product tight framelet* TP-$\mathbb{C}$TF$_6$*. All the first four columns use the same bivariate shrinkage developed in* [35]*. The last two columns use the Gaussian scale mixture in* [30]*. Gain refers to the PSNR gain of the current column over* DT-$\mathbb{C}$WT *in column* 2.

	Lena (512×512)					
σ_n	DT-$\mathbb{C}$WT	TP-$\mathbb{C}$TF$_3$	TP-$\mathbb{C}$TF$_4$	TP-$\mathbb{C}$TF$_6$ (Gain)	$\mathbb{C}$TF$_4$-GSM	$\mathbb{C}$TF$_6$-GSM (Gain)
5	38.25	37.96	38.10	**38.35** (0.10)	38.43	**38.53** (0.28)
10	35.19	34.91	35.14	**35.45** (0.26)	35.59	**35.70** (0.51)
15	33.47	33.25	33.50	**33.77** (0.30)	33.88	**34.01** (0.54)
20	32.23	32.07	32.31	**32.55** (0.22)	32.63	**32.77** (0.54)
25	31.26	31.15	31.38	**31.58** (0.32)	31.62	**31.78** (0.56)
30	30.47	30.40	30.61	**30.78** (0.31)	30.79	**30.96** (0.49)
50	28.21	28.29	28.41	**28.50** (0.29)	28.49	**28.64** (0.43)

Table 3

Denoising results for 512×512 *Barbara image.*

	Barbara (512×512)					
σ_n	DT-$\mathbb{C}$WT	TP-$\mathbb{C}$TF$_3$	TP-$\mathbb{C}$TF$_4$	TP-$\mathbb{C}$TF$_6$ (Gain)	$\mathbb{C}$TF$_4$-GSM	$\mathbb{C}$TF$_6$-GSM (Gain)
5	37.36	37.16	37.41	**37.82** (0.46)	37.75	**38.10** (0.74)
10	33.52	33.17	33.62	**34.14** (0.48)	34.10	**34.47** (0.95)
15	31.38	30.89	31.47	**32.02** (0.64)	31.97	**32.32** (0.94)
20	29.87	29.27	29.91	**30.49** (0.62)	30.43	**30.77** (0.90)
25	28.70	28.01	28.71	**29.31** (0.61)	29.26	**29.57** (0.87)
30	27.77	27.01	27.74	**28.34** (0.57)	28.32	**28.61** (0.84)
50	25.26	24.51	25.21	**25.71** (0.45)	25.69	**26.02** (0.76)

Table 4

Denoising results for 512×512 *Boat image.*

	Boat (512×512)					
σ_n	DT-$\mathbb{C}$WT	TP-$\mathbb{C}$TF$_3$	TP-$\mathbb{C}$TF$_4$	TP-$\mathbb{C}$TF$_6$ (Gain)	$\mathbb{C}$TF$_4$-GSM	$\mathbb{C}$TF$_6$-GSM (Gain)
5	36.77	36.44	36.52	**36.90** (0.13)	36.90	**37.07** (0.30)
10	33.21	32.96	33.08	**33.39** (0.17)	33.57	**33.69** (0.48)
15	31.33	31.15	31.28	**31.53** (0.20)	31.69	**31.81** (0.48)
20	30.01	29.91	30.01	**30.22** (0.21)	30.35	**30.48** (0.47)
25	28.99	28.94	29.03	**29.22** (0.23)	29.33	**29.46** (0.47)
30	28.18	28.16	28.22	**28.41** (0.23)	28.51	**28.63** (0.45)
50	26.01	26.00	26.04	**26.19** (0.18)	26.27	**26.39** (0.38)

for tree one and $\{a^2; b^2\}$ for tree two, instead of $\{a^0; b^0\}$ for tree one and $\{a^0(\cdot - 1); b^0(\cdot - 1)\}$ for tree two as proposed in [34] (see section 2). Note that for the approach in [24, 25] we have $\widehat{a^2}(\xi)/\widehat{a^1}(\xi) \approx e^{-i\xi/2}$ (that is, half-shift difference between tree two and tree one) while for the approach in [34] $\widehat{a^0(\cdot - 1)}(\xi)/\widehat{a^0}(\xi) = e^{-i\xi}$ (full-shift difference).

In the function setting, there is no difference between these two approaches. Indeed, the

Table 5
Denoising results for 256×256 *House image.*

	House (256×256)					
σ_n	DT-$\mathbb{C}$WT	TP-$\mathbb{C}$TF$_3$	TP-$\mathbb{C}$TF$_4$	TP-$\mathbb{C}$TF$_6$ (Gain)	$\mathbb{C}$TF$_4$-GSM	$\mathbb{C}$TF$_6$-GSM (Gain)
5	38.45	38.40	38.54	**38.91** (0.46)	38.82	**39.13** (0.68)
10	34.78	34.76	34.94	**35.43** (0.65)	35.42	**35.77** (0.99)
15	32.90	32.97	33.13	**33.57** (0.67)	33.65	**33.99** (1.09)
20	31.63	31.76	31.90	**32.32** (0.69)	32.36	**32.72** (1.09)
25	30.65	30.81	30.94	**31.34** (0.69)	31.34	**31.69** (1.04)
30	29.84	30.04	30.15	**30.52** (0.68)	30.49	**30.82** (0.98)
50	27.57	27.89	27.90	**28.14** (0.57)	28.11	**28.36** (0.79)

Table 6
Denoising results for 256×256 *Pepper image.*

	Pepper (256×256)					
σ_n	DT-$\mathbb{C}$WT	TP-$\mathbb{C}$TF$_3$	TP-$\mathbb{C}$TF$_4$	TP-$\mathbb{C}$TF$_6$ (Gain)	$\mathbb{C}$TF$_4$-GSM	$\mathbb{C}$TF$_6$-GSM (Gain)
5	37.18	36.98	37.07	**37.25** (0.07)	37.55	**37.61** (0.43)
10	33.40	33.29	33.41	**33.61** (0.21)	34.02	**34.07** (0.67)
15	31.29	31.28	31.38	**31.60** (0.31)	31.93	**32.01** (0.72)
20	29.83	29.90	29.96	**30.20** (0.37)	30.42	**30.54** (0.71)
25	28.71	28.82	28.86	**29.11** (0.40)	29.27	**29.43** (0.72)
30	27.80	27.95	27.97	**28.23** (0.43)	28.34	**28.53** (0.73)
50	25.30	25.52	25.51	**25.77** (0.47)	25.80	**26.02** (0.72)

refinable functions for the approach in [34] (that is, section 2) are

$$\begin{aligned}\widehat{\phi^1}(\xi) := \lim_{J\to\infty} 2^{(1-J)/2}\widehat{a^1_J}(2^{-J}\xi) &= \lim_{J\to\infty} \widehat{a^1}(2^{-1}\xi)\cdots\widehat{a^1}(2^{1-J}\xi)\widehat{a^0}(2^{-J}\xi)\\ &= \prod_{j=1}^{\infty}\widehat{a^1}(2^{-j}\xi) =: \widehat{\phi^{a^1}}(\xi)\end{aligned}$$

and, similarly,

$$\begin{aligned}\widehat{\phi^2}(\xi) := \lim_{J\to\infty} 2^{(1-J)/2}\widehat{a^2_J}(2^{-J}\xi) &= \lim_{J\to\infty} \widehat{a^2}(2^{-1}\xi)\cdots\widehat{a^2}(2^{1-J}\xi)\widehat{a^0(\cdot-1)}(2^{-J}\xi)\\ &= \prod_{j=1}^{\infty}\widehat{a^2}(2^{-j}\xi) =: \widehat{\phi^{a^2}}(\xi).\end{aligned}$$

That is, $\phi^1 = \phi^{a^1}$ and $\phi^2 = \phi^{a^2}$. Consequently, the half-shift condition in (2.8) implies

$$\widehat{\phi^{a^2}}(\xi) \approx e^{-i\xi/2}\widehat{\phi^{a^1}}(\xi) \quad \text{and} \quad \widehat{\phi^2}(\xi) \approx e^{-i\xi/2}\widehat{\phi^1}(\xi).$$

Define ψ^1 and ψ^2 by $\widehat{\psi^1}(\xi) := \widehat{b^1}(\xi/2)\widehat{\phi^{a^1}}(\xi/2)$ and $\widehat{\psi^2}(\xi) := \widehat{b^2}(\xi/2)\widehat{\phi^{a^2}}(\xi/2)$. Now it follows from the relation in (2.10) that

$$\widehat{\psi^2}(2\xi) = \widehat{b^2}(\xi)\widehat{\phi^{a^2}}(\xi) \approx -i\,\mathrm{sgn}(\xi)e^{i\xi/2}\widehat{b^1}(\xi)e^{-i\xi/2}\widehat{\phi^{a^1}}(\xi) = -i\,\mathrm{sgn}(\xi)\widehat{\psi^1}(2\xi).$$

(a) Original image

(b) Noisy image

(c) By DT-$\mathbb{C}$WT

(d) By TP-$\mathbb{C}$TF$_6$

(e) By TP-$\mathbb{C}$TF$_6$ and GSM

Figure 9. (a) *Original* 512×512 *image of Lena.* (b) *Noisy image with* $\sigma_n = 30$ *(PSNR* $= 18.60$*).* (c) *Denoised image by* DT-$\mathbb{C}$WT *(PSNR* $= 30.47$*).* (d) *Denoised image by* TP-$\mathbb{C}$TF$_6$ *using bivariate shrinkage (PSNR* $= 30.76$*).* (e) *Denoised image by* TP-$\mathbb{C}$TF$_6$ *using Gaussian scale mixture (PSNR* $= 30.94$*).*

Therefore, the Hilbert transform relation in the function setting still holds for both approaches. However, in terms of discrete affine systems, which faithfully reflect the dual tree complex wavelet transform, these two approaches have nontrivial differences.

Let us first consider level $j \ge 2$ by replacing $\{a^0; b^0\}$ and $\{a^0(\cdot - 1); b^0(\cdot - 1)\}$ with $\{a^1; b^1\}$ and $\{a^2; b^2\}$, respectively. In this case, (2.13) and (2.14) become

$$\widehat{\mathring{a}^1_j}(\xi) := 2^{(j-1)/2}\widehat{a^1}(\xi)\widehat{a^1}(2\xi)\cdots\widehat{a^1}(2^{j-1}\xi), \quad \widehat{\mathring{a}^2_j}(\xi) := 2^{(j-1)/2}\widehat{a^2}(\xi)\widehat{a^2}(2\xi)\cdots\widehat{a^2}(2^{j-1}\xi),$$

where we added a small circle over the multilevel filters for the approach in [24, 25] to distinguish them from the corresponding multilevel filters in [34] (see section 2); e.g., the above multilevel filters $\mathring{a}^1_j$ and $\mathring{a}^2_j$ used in the approach in [24, 25] correspond to the multilevel filters a^1_j and a^2_j that we discussed in section 2, respectively.

Then by the half-shift condition in (2.8), we have

$$\widehat{\mathring{a}^2_j}(2^{-j}\xi) \approx \widehat{\mathring{a}^1_j}(2^{-j}\xi)e^{-i2^{-j-1}\xi}e^{i\sum_{\ell=1}^{j-1}\theta(2^{-\ell}\xi)}.$$

That is, we lost a factor $e^{-i2^{-j-1}\xi}$ in (2.19), or equivalently, the above is obtained by multiplying $e^{i2^{-j-1}\xi}$ to (2.19). Consequently, the same analysis as in section 2 shows that (2.21)

(a) Original image

(b) Noisy image

(c) By DT-$\mathbb{C}$WT

(d) By TP-$\mathbb{C}$TF$_6$

(e) By TP-$\mathbb{C}$TF$_6$ and GSM

Figure 10. (a) *Original* 512×512 *image of Barbara.* (b) *Noisy image with* $\sigma_n = 20$ *(PSNR* $= 22.12$*).* (c) *Denoised image by* DT-$\mathbb{C}$WT *(PSNR* $= 29.85$*).* (d) *Denoised image by* TP-$\mathbb{C}$TF$_6$ *using bivariate shrinkage (PSNR* $= 30.48$*).* (e) *Denoised image by* TP-$\mathbb{C}$TF$_6$ *using Gaussian scale mixture (PSNR* $= 30.75$*).*

now becomes

$$\widehat{\mathring{a}_j^2}(\xi) \approx e^{-i2^{j-1}\xi} e^{i\xi/2} \widehat{\mathring{a}_j^1}(\xi)\eta(2^j\xi) \approx e^{-i2^{j-1}\xi} e^{i\xi/2} \widehat{\mathring{a}_j^1}(\xi), \qquad \xi \in [-\pi,\pi), j \ge 2,$$

which implies $\mathring{a}_j^2 \approx \mathring{a}_j^1(\cdot - 2^{j-1} + 1/2)$ in the time domain. For the low-pass filters in (2.23), we have

$$\widehat{\mathring{a}_j^p}(\xi) = [\widehat{\mathring{a}_j^1}(\xi) + i\widehat{\mathring{a}_j^2}(\xi)]/\sqrt{2} \approx \widehat{\mathring{a}_j^1}(\xi)[1 + ie^{-i2^{j-1}\xi + i\xi/2}]/\sqrt{2}, \qquad \xi \in [-\pi,\pi).$$

Since $|\widehat{\mathring{a}_j^1}(\xi)| \approx 2^{j-1}\chi_{2^{-j}[-\pi,\pi)}$ for $\xi \in [-\pi,\pi)$ and $|1+ie^{-i2^{j-1}\xi+i\xi/2}|^2 = 2+2\sin(2^{j-1}\xi - 2^{-1}\xi)$, we have

$$\begin{aligned} |\widehat{\mathring{a}_j^p}(\xi)| &\approx \sqrt{1+\sin(2^{j-1}\xi - 2^{-1}\xi)}\,|\widehat{\mathring{a}_j^1}(\xi)| \\ &\approx \sqrt{1+\sin(2^{j-1}\xi - 2^{-1}\xi)}\,2^{(j-1)/2}\chi_{2^{-j}[-\pi,\pi)}(\xi), \qquad \xi \in [-\pi,\pi). \end{aligned}$$

When j is large, the frequency separation factor $\sqrt{1+\sin(2^{j-1}\xi - 2^{-1}\xi)} \approx \sqrt{1+\sin(2^{j-1}\xi)}$ is more or less the same as in (2.26) on $\xi \in 2^{-j}[-\pi,\pi)$. But when j is small (in particular,

$j = 2$ and 3), by plotting and comparing these functions, we see that the frequency separation factor $\sqrt{1+\sin(2^{j-1}\xi - 2^{-1}\xi)}$ is always slightly worse than the frequency separation factor $\sqrt{1+\sin(2^{j-1}\xi)}$ on the interval $2^{-j}[-\pi,\pi)$.

For high-pass filters, (2.22) becomes

$$\mathring{\widehat{b}}{}_j^p(\xi) := [\mathring{\widehat{b}}{}_j^1(\xi) + i\mathring{\widehat{b}}{}_j^2(\xi)]/\sqrt{2} = \mathring{\widehat{b}}{}_j^1(\xi)[1 + e^{i\xi/2}\operatorname{sgn}(\xi)]/\sqrt{2}.$$

Note that

$$|[1 + e^{i\xi/2}\operatorname{sgn}(\xi)]/\sqrt{2}| = \sqrt{1+\cos(\xi/2)\operatorname{sgn}(\xi)} = \begin{cases} \sqrt{1+\cos(\xi/2)} & \text{if } \xi \in [0,\pi), \\ \sqrt{1-\cos(\xi/2)} & \text{if } \xi \in [-\pi,0). \end{cases} \tag{5.1}$$

For the approach in section 2 (that is, [34]), for $j \ge 2$, we have the ideal frequency separation in (2.22), that is, $\widehat{b}_j^p \approx \sqrt{2}\widehat{b}_j^1\chi_{[0,\pi)}$ and $\widehat{b}_j^n \approx \sqrt{2}\widehat{b}_j^1\chi_{[-\pi,0)}$ on the basic frequency interval $[-\pi,\pi)$. That is, we are using the ideal frequency separation factor $\sqrt{2}\chi_{[0,\pi)}$ for the approach in section 2 when $j \ge 2$. But the frequency separation factor in (5.1) is not ideal and is much worse than the ideal frequency separation factor when j is small. However, in every application, directionality for small decomposition levels is much more important. When the decomposition level J increases, the resolution of the processed image decreases by a factor of 2 (the processed image at decomposition level J becomes smoother when J becomes larger). However, it is very natural that when the resolution level is higher, we need more and better directions. In this sense, for level $J \ge 2$, the approach proposed in [34] has better directionality than the original approach of Kingsbury [24, 25].

Let us now consider level one. Then we have

$$\mathring{a}_1^p := [a^1 + ia^2]/\sqrt{2}, \quad \mathring{a}_1^n := [a^1 - ia^2]/\sqrt{2}, \quad \text{and} \quad \mathring{b}_1^p := [b^1 + ib^2]/\sqrt{2}, \quad \mathring{b}_1^n := [b^1 - ib^2]/\sqrt{2}.$$

For low-pass filters, we have

$$\mathring{\widehat{a}}{}_1^p(\xi) = [\widehat{a^1}(\xi) + i\widehat{a^2}(\xi)]/\sqrt{2} \approx \widehat{a^1}(\xi)[1 + ie^{-i\xi/2}]/\sqrt{2}, \qquad \xi \in [-\pi,\pi).$$

By $|1 + ie^{-i\xi/2}| = 2 + \sin(\xi/2)$, we have

$$|\mathring{\widehat{a}}{}_1^p(\xi)| \approx \sqrt{1+\sin(\xi/2)}|\widehat{a^1}(\xi)|, \qquad \xi \in [-\pi,\pi). \tag{5.2}$$

See Figure 11 for graphs of the several frequency separation factors. From the graphs in Figure 11, since $|\widehat{a^1}|^2 \approx \chi_{[-\pi/2,\pi/2]}$ for $\xi \in [-\pi,\pi)$, we see that the frequency separation factor $\sqrt{1+\sin(\xi/2)}$ is slightly worse than the frequency separation factor $\sqrt{1+\sin\xi}$ for splitting the low-pass filter a^1.

For high-pass filters, we have

$$\begin{aligned} \mathring{\widehat{b}}{}_1^p(\xi) &= [\widehat{b^1}(\xi) + i\widehat{b^2}(\xi)]/\sqrt{2} = [e^{-i\xi}\overline{\widehat{a^1}(\xi+\pi)} + ie^{-i\xi}\overline{\widehat{a^2}(\xi+\pi)}]/\sqrt{2} \\ &\approx e^{-i\xi}\overline{\widehat{a^1}(\xi+\pi)}[1 + ie^{-i\theta(\xi+\pi)}]/\sqrt{2}. \end{aligned}$$

Since

$$e^{-i\theta(\xi+\pi)} = e^{i(\xi+\pi)/2}e^{-i\pi\lfloor\frac{\xi+2\pi}{2\pi}\rfloor} = e^{i\xi/2}e^{i\pi\lfloor\frac{\xi}{2\pi}\rfloor} = \operatorname{sgn}(\xi)e^{i\xi/2}$$

for $\xi \in (-2\pi, 2\pi)$, we conclude that

$$\widehat{\mathring{b}_1^p}(\xi) \approx \widehat{b^1}(\xi)[1 + e^{i\xi/2}\operatorname{sgn}(\xi)]/\sqrt{2}, \qquad \xi \in [-\pi, \pi).$$

Now we see that the above frequency separation factor is the same as in (5.1) for $j \geq 2$. Since $|\widehat{b^1}|^2 \approx 2^{j-1}\chi_{[-\pi,-\pi/2]\cup[\pi/2,\pi]}$ on $[-\pi, \pi)$, from Figure 11, we see that the frequency separator factor in (5.1) for $j = 1$ is slightly worse than the frequency separation factor $\sqrt{1+\sin\xi}$ for $\xi \in [-\pi, \pi)$ in (2.17) for splitting the high-pass filter b^1. Moreover, by (5.1) and $|\widehat{a^1}(\xi)|^2 + |\widehat{a^1}(\xi+\pi)|^2 = 1$, we deduce that

$$\begin{aligned}\int_0^\pi \big[|\widehat{b_1^p}(\xi+\pi)|^2 + |\widehat{b_1^n}(\xi)|^2\big]d\xi &\approx \int_0^\pi \big[|\widehat{a^1}(\xi)|^2(1-\sin(\xi/2)) + |\widehat{a^1}(\xi+\pi)|^2(1-\cos(\xi/2))\big]d\xi \\ &= \pi - \int_{-\pi}^\pi |\widehat{a^1}(\xi)|^2|\sin(\xi/2)|d\xi \approx \pi - \int_{-\pi/2}^{\pi/2}|\sin(\xi/2)|d\xi = \pi - (4-2\sqrt{2}) > \pi - 2.\end{aligned}$$

Comparing with (2.18), the directionality for level one using the approach in [24, 25] is slightly worse than the approach in [34]. In conclusion, we see that the approach in [34] has slightly better directionality than the approach in [24, 25].

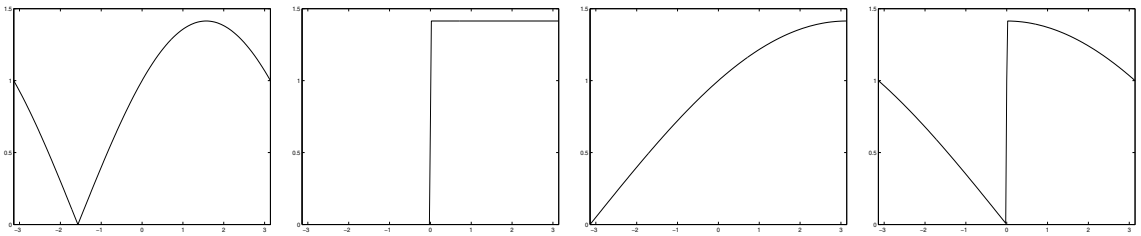

(a) (b) (c) (d)

Figure 11. (a) *The frequency separation factor* $\sqrt{1+\sin\xi}$ *in* (2.17), (b) *the ideal frequency separation factor* $(1+\operatorname{sgn}(\xi))/\sqrt{2}$ *in* (2.22), (c) *the frequency separation factor* $\sqrt{1+\sin(\xi/2)}$ *in* (5.2), *and* (d) *the frequency separation factor* $\sqrt{1+\cos(\xi/2)\operatorname{sgn}(\xi)}$ *in* (5.1). *Note that* $\int_{-\pi}^{\pi}|\sqrt{1+\sin\xi}|^2d\xi = \int_{-\pi}^{\pi}|(1+\operatorname{sgn}(\xi))/\sqrt{2}|^2d\xi = \int_{-\pi}^{\pi}|\sqrt{1+\sin(\xi/2)}|^2d\xi = \int_{-\pi}^{\pi}|\sqrt{1+\cos(\xi/2)\operatorname{sgn}(\xi)}|^2d\xi = 2\pi$.

However, as we pointed out in (2.18) of section 2, the directionality for the first level of the DT-$\mathbb{C}$WT is not very strong. To remedy this shortcoming, we can replace the initial tight framelet filter bank $2^{-1/2}\{a^0, a^0(\cdot-1); b^1, b^2\}$ by the undecimated version of tensor product complex tight framelet filter bank TP-$\mathbb{C}$TF$_n$ with n relatively large; more precisely, we use the following tight framelet filter bank as the initial filter bank in the DT-$\mathbb{C}$WT:

$$2^{-1/2}\{a, a(\cdot-1); b^{1,p}, \ldots, b^{s,p}, b^{1,n}, \ldots, b^{s,n}, b^{1,p}(\cdot-1), \ldots, b^{s,p}(\cdot-1), b^{1,n}(\cdot-1), \ldots, b^{s,n}(\cdot-1)\}.$$

Their performance on image denoising is reported in Table 7. We can see the improvement due to more directions in the first stage filter bank, especially when the image contains many

details such as Barbara. Since the directions are not the same between the first level and the second level, the coefficients along approximately the same direction share a common parent. When the noise level is high, the parent coefficients can only provide information to predict the threshold value on the same direction as the child coefficients. Also, when the noise level is high, most uncorrupted high-pass wavelet coefficients at the finest scale cannot be distinguished from the noise and consequently are reduced to zero by thresholding. These are the two main reasons for the limited or no improvement of the PSNR values for high noise level.

Table 7

Columns of ℂWT *are for PSNR values (an average over five experiments) using bivariate shrinkage in* [36] *and the* DT-ℂWT *using finitely supported orthogonal wavelet filter banks in* (3.1)–(3.3). *Columns of* NℂWT *are for PSNR values using the same bivariate shrinkage and then the* DT-ℂWT, *except that the first level transform uses the tight framelet filter bank* TP-$\mathbb{C}\mathrm{TF}_6$ *(*14 *directions) instead of the filter bank in* (3.1).

	Lena		Barbara		Boat		House		Pepper	
σ_n	ℂWT	NℂWT	ℂWT	NℂWT	ℂWT	NℂWT	ℂWT	NℂWT	ℂWT	NℂWT
5	38.25	38.27	37.36	37.73	36.77	36.70	38.45	38.67	37.18	37.19
10	35.19	35.35	33.52	33.96	33.21	33.28	34.78	35.05	33.40	33.50
15	33.47	33.61	31.38	31.73	31.33	31.36	32.90	33.16	31.29	31.36
20	32.23	32.34	29.87	30.13	30.01	30.00	31.63	31.80	29.83	29.85
25	31.26	31.34	28.70	28.90	28.99	28.96	30.65	30.74	28.71	28.71
30	30.47	30.52	27.77	27.90	28.18	28.14	29.84	29.88	27.80	27.78
50	28.21	28.24	25.26	25.27	26.01	25.97	27.57	27.53	25.30	25.27

We point out that the issue of improving directionality for the first level of the DT-ℂWT has also been addressed in [11]. The key ingredient of the approach in [11] is to replace the filter bank $\{a^0(\cdot-1); b^0(\cdot-1)\}$ for tree two in the first level by another filter bank $\{a^0(\cdot-1); \breve{b})$, where $\widehat{\breve{b}}(\xi) := e^{-i\xi}\widehat{b}(\xi)\widehat{Q}(\xi)$ such that $|\widehat{Q}(\xi)| = 1$ and $\widehat{Q}(\xi+\pi) = \widehat{Q}(\xi)$ for all $\xi \in \mathbb{R}$. Due to the conditions on Q, it is trivial to check that $\{a^0(\cdot-1); \breve{b})$ is still an orthogonal wavelet filter bank. In short, the approach in [11] improves the directionality of the first level of the DT-ℂWT by adding an appropriate phase factor to the high-pass filter $b^0(\cdot-1)$ for tree two. Due to the conditions on the filter Q, as pointed out in [11], Q cannot be a finitely supported filter.

6. Relations with other wavelet-based directional representations. In this section, we shall discuss the relations of our approach of tensor product complex tight framelets with other recent advances in wavelet-based directional representations such as generalizations of the DT-ℂWT [1, 4], shearlets [22, 26, 27, 28], and directional nonseparable tight framelets [18]. We shall also compare the performance of TP-ℂTFs with the image denoising results by shearlets reported in [27, 28].

6.1. Relations to generalizations of the DT-ℂWT. Among several generalizations of the DT-ℂWT, two major generalizations of the DT-ℂWT are the dual tree complex M-band wavelet transform (M-band DT-ℂWT) in [4] and the dual tree complex wavelet packet transform (DT-ℂWPT) in [1].

Except variants of the Haar orthogonal wavelet, it is well known [5] that there are no compactly supported symmetric real-valued 2-band orthogonal wavelets. The main advantage

of M-band wavelets is symmetry since compactly supported real-valued M-band orthogonal wavelets can achieve symmetry when $M > 2$. As discussed in [4], this advantage of symmetry carries over to the M-band DT-$\mathbb{C}$WT. Though the extension of the (2-band) DT-$\mathbb{C}$WT to the M-band DT-$\mathbb{C}$WT offers several new features and flexibilities, there are several difficulties hindering their developments and applications. First, using a dilation factor $M > 2$, the level/depth of the wavelet tree is often significantly reduced since M-band wavelets employ the downsampling factor M instead of 2. With more intermediate levels for $M = 2$, one has more flexibility for better processing wavelet coefficients by exploring the cross-scale (or interscale) dependency/relation. Second, it is far from trivial to construct smooth compactly supported symmetric real-valued M-band orthogonal refinable functions. In fact, there are only a few such known examples in the literature; see, e.g., [14] for a systematic construction of compactly supported symmetric real-valued M-band orthogonal refinable functions. Third, in contrast to the case of $M = 2$ (see (2.7)), for $M > 2$, it is much harder to derive symmetric M-band orthogonal wavelets from symmetric M-band orthogonal refinable functions. This problem is a special case of the matrix extension problem with symmetry, which has been systematically studied and solved in [15]. Even though one can use the general algorithm in [15] or the particular method in [14] for special cases to construct symmetric M-band orthogonal wavelets from symmetric M-band orthogonal refinable functions, to have the M-band DT-$\mathbb{C}$WT, it is still far from trivial for the constructed wavelet functions to satisfy the required condition in (1.4) for approximate Hilbert-transform pairs. In fact, our approach TP-$\mathbb{C}$TFs can easily be generalized to the case of $M \geq 2$. Due to the first mentioned difficulty for M-band wavelets, we consider only TP-$\mathbb{C}$TFs with $M = 2$ in this paper. In fact, the low-pass filters in TP-$\mathbb{C}$TFs with $M = 2$ can easily achieve symmetry since every symmetric low-pass filter a satisfying $|\widehat{a}(\xi)|^2 + |\widehat{a}(\xi + \pi)|^2 \leq 1$ can be used to construct TP-$\mathbb{C}$TFs. Moreover, with the recent development in complex tight framelets in [20, 21], it is much easier to construct compactly supported symmetric complex tight framelets than symmetric M-band orthogonal wavelets.

Another generalization of the DT-$\mathbb{C}$WT is the dual tree complex (M-band) wavelet packet transform (DT-$\mathbb{C}$WPT). By recursively applying the wavelet transform to all wavelet coefficients instead of only those from the low-pass filter, wavelet packets offer more choices of bases and consequently could have better performance than classical wavelets by finding the best possible choice of wavelet packet bases for a given data. Using the idea of wavelet packets, [1] generalized the DT-$\mathbb{C}$WT to the DT-$\mathbb{C}$WPT, which inherits the advantages of wavelet packets and improves the directionality of the DT-$\mathbb{C}$WT. The idea of wavelet packets can obviously be applied to TP-$\mathbb{C}$TFs as well. However, due to the recursive application of the wavelet transform on all wavelet coefficients, wavelet packets and the DT-$\mathbb{C}$WPT partition the frequency band of a high-pass filter into smaller and smaller frequency bands (e.g., see [1, Figure 1]). As a consequence, the filters in the discrete affine systems of the DT-$\mathbb{C}$WPT become less localized in the spatial domain. On the other hand, the TP-$\mathbb{C}$TFs do not extensively split the frequency bands and therefore lead to better spatial localization. This partially explains (also see the following subsection) why the graphs in Figure 8 have better spatial localization than those of the DT-$\mathbb{C}$WPT in [1, Figure 12]. Moreover, the relations among cross-scale (or interscale) wavelet coefficients may be lost in wavelet packets and the DT-$\mathbb{C}$WPT. But such relations play a key role in the bivariate shrinkage used in [35, 36] for image denoising.

6.2. Directionality of complex-valued functions and filters. It is important for us to understand how and why tensor product complex wavelets/framelets such as the DT-$\mathbb{C}$WT, the DT-$\mathbb{C}$WPT, and the TP-$\mathbb{C}$TFs can achieve directionality in high dimensions. In the following, we discuss complex-valued wavelet functions $\psi : \mathbb{R}^2 \to \mathbb{C}$. The same argument can be applied to high-pass filters $b : \mathbb{Z}^2 \to \mathbb{C}$ as well. Separating the real and imaginary parts of ψ, we have $\psi = \psi^{[r]} + i\psi^{[i]}$, where $\psi^{[r]}$ and $\psi^{[i]}$ are real-valued two-dimensional functions. For $\psi^{[r]}$ and $\psi^{[i]}$ to have directionality, $\widehat{\psi}$ often concentrates near a point (i.e., a nonzero vector) $\zeta \in \mathbb{R}^2\backslash\{0\}$ in the frequency domain. More precisely, $\widehat{\psi}(\xi) = g(\xi - \zeta)$, where g is a function concentrating around the origin. Let f be the inverse Fourier transform of g, that is, $\widehat{f} = g$. For the DT-$\mathbb{C}$WT and the TP-$\mathbb{C}$TFs, f is often a real-valued isotropic function concentrating around the origin. Now we deduce from the relation $\widehat{\psi}(\xi) = g(\xi - \zeta) = \widehat{f}(\xi - \zeta)$ that

$$\psi(x) = f(x)e^{i\zeta\cdot x} \quad \text{and} \quad \psi^{[r]}(x) = f(x)\cos(\zeta \cdot x), \quad \psi^{[i]}(x) = f(x)\sin(\zeta \cdot x)\ \forall\, x \in \mathbb{R}^2. \tag{6.1}$$

Even though the complex-valued function ψ has isotropic magnitude $|\psi(x)| = |f(x)|$ and does not have any directionality at all, its real part $\psi^{[r]}$ and its imaginary part $\psi^{[i]}$ indeed have directionality, due to the directionality of $\cos(\zeta \cdot x)$ and $\sin(\zeta \cdot x)$ (provided $\zeta \neq 0$). On one hand, the function f provides a good spatial localization and magnitude for $\psi^{[r]}$ and $\psi^{[i]}$. On the other hand, the factors $\cos(\zeta \cdot x)$ and $\sin(\zeta \cdot x)$ provide directionality for $\psi^{[r]}$ and $\psi^{[i]}$. Note that $\psi^{[r]}$ and $\psi^{[i]}$ have the same direction, which is perpendicular to the vector ζ. When $\|\zeta\|$ is larger, the frequency of $\cos(\zeta \cdot x)$ and $\sin(\zeta \cdot x)$ is higher and therefore, there are more oscillations in $\psi^{[r]}$ and $\psi^{[i]}$ per unit in the direction of ζ. For the DT-$\mathbb{C}$WPT, the wavelet functions ψ often have smaller frequency localization than those in TP-$\mathbb{C}$TFs. As a consequence, the function f (i.e., the magnitude of ψ) will have more spread-out and worse spatial localization, which may not be desired in applications. On the other hand, TP-$\mathbb{C}$TFs can easily achieve an effect similar to that in the DT-$\mathbb{C}$WPT, that is, having more texture-like (i.e., more oscillations) elements by using a larger number of high-pass filters.

We now explain the directionality and oscillations for the graphs in Figure 8. Note that the corresponding vectors ζ of the complex wavelet functions associated with the 12 high-pass filters in $\{a^p, a^n; b^{1,p}, b^{1,n}\} \otimes \{a^p, a^n; b^{1,p}, b^{1,n}\}$ (but excluding the four low-pass filters in $\{a^p, a^n\} \otimes \{a^p, a^n\}$) have small norms and total six different nonzero vectors. Therefore, the graphs of the real and imaginary parts of these complex-valued wavelet functions/filters exhibit six edge-like (i.e., fewer oscillations) directions in Figure 8. On the other hand, the corresponding vectors ζ of the complex wavelet functions associated with all other 20 high-pass filters in TP-$\mathbb{C}$TF-HP$_6$ have larger norms and total 10 different directions (two of them are directions along $\pm 45°$). Therefore, the graphs of the real and imaginary parts of these complex-valued wavelet functions/filters exhibit 10 texture-like (i.e., more oscillations) directions in Figure 8. The good performance of TP-$\mathbb{C}$TF$_6$ for image denoising is probably due to the fact that TP-$\mathbb{C}$TF$_6$ has both edge-like directional elements (for capturing edges) and texture-like directional elements (for capturing textures).

6.3. Relations to shearlets and directional nonseparable tight framelets. There are several recent developments in wavelet-based directional representations. Here we discuss only two of them: the well-known approach of (cone-based) shearlets (see [8, 9, 12, 22, 26, 27, 28] and many references therein) and the approach of directional nonseparable tight framelets in

[18].

Let U be a $d \times d$ real-valued invertible matrix and $f : \mathbb{R}^d \to \mathbb{C}$ be a function. Following [18], we shall adopt the following notation in this subsection:

$$f_{U;k,n}(x) := [\![U;k,n]\!]f(x) := |\det U|^{1/2} e^{-in\cdot Ux} f(Ux-k) \quad \text{and} \quad f_{U;k} := f_{U;k,0}, \qquad x,k,n \in \mathbb{R}^d.$$

To give the reader some ideas about (cone-based) shearlets, let us recall the definition of (oversampled and cone-based) shearlets in dimension two (e.g., see [8, 9, 12, 26, 27, 28] and references therein). Define

$$A_{2^j} = \begin{bmatrix} 2^j & 0 \\ 0 & 2^{\lfloor j/2 \rfloor} \end{bmatrix}, \quad S := \begin{bmatrix} 1 & 1 \\ 0 & 1 \end{bmatrix}, \quad C := \begin{bmatrix} c_1 & 0 \\ 0 & c_2 \end{bmatrix} \quad \text{with} \quad c_1, c_2 > 0.$$

A_{2^j} are the hyperbolic dilation matrices, S is the shear matrix, and C is the oversampling matrix (for original shearlets, $C = I_2$ with $c_1 = c_2 = 1$). Let φ and ψ be functions in $L_2(\mathbb{R}^2)$. Then a cone-based over-sampled shearlet system is defined to be

$$\begin{aligned} \mathrm{CSH}(\varphi;\psi) :=& \{\varphi_{I_2;c_1 k} \ : \ k \in \mathbb{Z}^2\} \\ & \cup \{\psi_{S^\ell A_{2^j};Ck}, E(\psi_{S^\ell A_{2^j};Ck}) \ : \ j \ge 0, \ell = -2^{\lceil j/2 \rceil}, \ldots, 2^{\lceil j/2 \rceil}, k \in \mathbb{Z}^2\}, \end{aligned}$$

where $E(f)(x,y) := f(y,x)$ for any two-dimensional function $f : \mathbb{R}^2 \to \mathbb{C}$ and $\lceil x \rceil = n$ for $n-1 < x \le n$ with $n \in \mathbb{Z}$. Now we explain how elements in $\mathrm{CSH}(\varphi;\psi)$ can achieve directionality. Note that

$$\mathrm{supp}(\psi_{S^\ell A_{2^j};Ck}) = A_{2^j}^{-1} S^{-\ell} Ck + A_{2^j}^{-1} S^{-\ell} \mathrm{supp}(\psi).$$

The function ψ is often constructed in a way that $\mathrm{supp}(\psi)$ has the vertical direction [8, 9, 12, 26, 27, 28]. Then $A_{2^j}^{-1} S^{-\ell} \mathrm{supp}(\psi)$ will be an elongated set with the direction along the line passing through the origin and having slope $-2^{j-\lfloor j/2 \rfloor}/\ell$. Therefore, the element $\psi_{S^\ell A_{2^j};Ck}$ has direction/slope $-2^{j-\lfloor j/2 \rfloor}/\ell$ with the spatial localization center $A_{2^j}^{-1} S^{-\ell} Ck$. Since $\ell = -2^{\lceil j/2 \rceil}, \ldots, 2^{\lceil j/2 \rceil}$, these elements at the level j provide good angular resolution for the vertical cone $\{(x,y)^{\mathsf{T}} \in \mathbb{R}^2 \ : \ |y| \ge |x|\}$. Using the operator E, we obtain directional elements for the horizontal cone.

Many interesting results on theory and application of shearlets have been reported in [8, 9, 12, 22, 26, 27, 28] and many references therein. By modifying the elements $\psi_{S^\ell A_{2^j};Ck}$ for $|\ell| \approx 2^{\lceil j/2 \rceil}$ (that is, elements having supports near the two seam lines $y = \pm x$) in $\mathrm{CSH}(\varphi;\psi)$, tight frames of shearlets for $L_2(\mathbb{R}^2)$ have been constructed in [12]. If continuous domain shearlets are used for digital data, to have a discrete transform, one has to calculate $\langle f, \psi_{S^\ell A_{2^j};Ck} \rangle$ in the continuum domain, where f is the function version of a given data. In [27], the approximation of $\langle f, \psi_{S^\ell A_{2^j};Ck} \rangle$ is achieved by using the pseudopolar Fourier transform for bandlimited shearlets. However, to achieve nearly perfect reconstruction property of the resulting discrete shearlet transform, the oversampling rate used in the pseudopolar Fourier transform is often very high, and this leads to a highly redundant discrete shearlet transform. Recently, Lim

[28] adopted the idea of wavelets with filter banks to efficiently approximate $\langle f, \psi_{S^\ell A_{2^j};Ck}\rangle$ by using a compactly supported function ψ which is built from wavelet functions and filters. As discussed in [28], with properly chosen compactly supported φ and ψ, CSH$(\varphi;\psi)$ can be a frame for $L_2(\mathbb{R}^2)$ by using small c_1, c_2 (leading to redundant shearlet systems). Mimicking the discrete wavelet transform using filter banks, the proposed discrete shearlet transform in [28] can be implemented using filter banks, but the reconstruction step uses functions and filters which are not compactly supported (see formulas (22) and (23) in [28]). Due to the approximation of $\langle f, \psi_{S^\ell A_{2^j};Ck}\rangle$, the proposed discrete shearlet transforms in [27, 28] can only have the nearly perfect reconstruction property. On the other hand, discrete domain shearlets employing multiresolution analysis and filter banks have been developed in [12]. The implementation of the shearlet transform in both the spatial domain and the frequency domain as well as their applications to image processing have been addressed in [8, 9]. TP-$\mathbb{C}$TFs in this paper directly use tensor product filter banks with the perfect reconstruction property but have only a preassigned number of directionality (this is intrinsic to any approach using the tensor product).

In the following, we compare the performance of our proposed approach TP-$\mathbb{C}$TFs with the image denoising results using shearlets in [27, 28]. Table 8 shows that the best possible image denoising results by compactly supported shearlets in [28] are comparable to those using the DT-$\mathbb{C}$WT, while the best possible image denoising results by bandlimited shearlets in [27] are inferior to those using the DT-$\mathbb{C}$WT. Both ShearLab-PPFT in [27] and DNST1 in [28] have much higher redundancy and are computationally more expensive (see [27, Tables 10 and 11] and [28, Figure 10]) than the DT-$\mathbb{C}$WT and TP-$\mathbb{C}$TF$_6$. Table 8 shows that the image denoising results using TP-$\mathbb{C}$TF$_6$ are better than the DT-$\mathbb{C}$WT in [36], ShearLab-PPFT in [27], and DNST1 in [28].

Table 8

Denoising results for 512×512 *test images of Lena and Barbara, which are used in* [28] *and from http://www.shearlet.org (but different from those used in sections 2–5). The denoising results in* [28] *using DNST*1 *(discrete nonseparable shearlet transform with* $8, 8, 16, 16$ *directions across scales) are from* [28, *Figure* 15]. *The denoising results in* [27] *using ShearLab-PPFT (shearlet transform using bandlimited shearlets and implemented using the fast pseudopolar Fourier transform) are from* [27, *Tables* 10 *and* 11]. *Note that the Barbara image used in* [27] *is not that from http://www.shearlet.org and is* 13 *pixel values less for almost every pixel than the Barbara image used in sections 2–5. Thus, the PSNR values for the* DT-$\mathbb{C}$WT, TP-$\mathbb{C}$TF$_6$, *and* $\mathbb{C}$TF$_6$*-GSM on the Barbara image used in* [27] *are the same as those in Table 3 and have at most* 0.05 *differences from the PSNR values in this table for* $\sigma_n = 20, 30, 40$.

	Lena (512×512)				
σ_n	DT-$\mathbb{C}$WT	TP-$\mathbb{C}$TF$_6$	$\mathbb{C}$TF$_6$-GSM	[27]	[28]
10	35.86	36.12	36.38	NA	35.90
20	32.59	32.89	33.13	31.32	32.75
30	30.72	31.01	31.21	29.38	30.84
40	29.39	29.67	29.84	28.07	29.41
	Barbara (512×512)				
σ_n	DT-$\mathbb{C}$WT	TP-$\mathbb{C}$TF$_6$	$\mathbb{C}$TF$_6$-GSM	[27]	[28]
10	33.80	34.22	34.48	NA	33.64
20	29.84	30.53	30.72	29.27	30.03
30	27.80	28.33	28.57	27.39	27.84
40	26.36	26.80	27.10	26.01	26.33

Let $\phi \in L_2(\mathbb{R}^d)$, and let Ψ be a finite subset of $L_2(\mathbb{R}^d)$. For every $J \in \mathbb{Z}$, an affine system is defined to be [18]

$$\mathsf{AS}_J(\phi;\Psi) := \{\phi_{2^J I_d;k} \ : \ k \in \mathbb{Z}^d\} \cup \{\psi_{2^j I_d;k} \ : \ j \geq J, k \in \mathbb{Z}^d, \psi \in \Psi\}. \tag{6.2}$$

As discussed in [18], if $\mathsf{AS}_0(\phi;\Psi)$ is a tight frame (or orthonormal basis) for $L_2(\mathbb{R}^d)$, then $\mathsf{AS}_J(\phi;\Psi)$ is a tight frame (or orthonormal basis) for $L_2(\mathbb{R}^d)$ for every $J \in \mathbb{Z}$. In other words, a tight frame $\mathsf{AS}_0(\phi;\Psi)$ induces a sequence $\{\mathsf{AS}_J(\phi;\Psi)\}_{J\in\mathbb{Z}}$ of tight frames at every scale level J. This sequence is closely linked to multiresolution analysis and filter banks ([18]). To have both directionality and filter banks, an approach of directional nonseparable tight framelets has been proposed in [18, Theorem 19]:

$$\mathsf{AS}_J(\phi;\{\Psi_j\}_{j=J}^\infty) := \{\phi_{2^J I_2;k} \ : \ k \in \mathbb{Z}^2\} \cup \cup_{j=J}^\infty \{\psi_{2^j I_2;k} \ : \ k \in \mathbb{Z}^2, \psi \in \Psi_j\}, \tag{6.3}$$

which are tight frames for $L_2(\mathbb{R}^2)$ for all $J \geq 0$. The elements in Ψ_j at scale level j have directionality and can be generated by one single function through rotation and scaling. Due to the increase of angular resolution when j is large, the number of elements in Ψ_j necessarily increases with the level j. More importantly, there is an underlying generalized tight framelet filter bank under the directional nonseparable tight framelet in (6.3). Comparing with TP-$\mathbb{C}$TFs, the tight framelet in [18] is nonseparable and has increasing directionality as $j \to \infty$, but its associated algorithm is not implemented yet. The idea of directional nonseparable tight framelets could be combined with TP-$\mathbb{C}$TFs to further enhance the performance of TP-$\mathbb{C}$TFs for having more edge-like directional elements.

6.4. Summary on tensor product complex tight framelets. We complete this paper by summarizing some properties of TP-$\mathbb{C}$TF$_n$ for further improvements. If one insists on using tensor product filter banks for high-dimensional problems, then the approach of TP-$\mathbb{C}$TF$_n$ with $n \geq 3$ is probably the most natural choice. For the convenience of the reader, we list some possible advantages of TP-$\mathbb{C}$TF$_n$ as follows:

(1) TP-$\mathbb{C}$TF$_n$ has more directions than the DT-$\mathbb{C}$WT when n increases.
(2) TP-$\mathbb{C}$TF$_n$ enjoys the same simple tensor product structure as the DT-$\mathbb{C}$WT. Therefore, its algorithm is essentially the same as the standard discrete wavelet transform using the tensor product.
(3) TP-$\mathbb{C}$TF$_4$ offers an alternative to the DT-$\mathbb{C}$WT while enjoying less redundancy than the DT-$\mathbb{C}$WT since TP-$\mathbb{C}$TF$_4$ uses only one low-pass filter and the DT-$\mathbb{C}$WT uses four low-pass filters for dimension two.
(4) The low-pass filters used in TP-$\mathbb{C}$TF$_n$ are not only real-valued but also have symmetry, which are desired in applications. In fact, every low-pass filter a satisfying $|\widehat{a}(\xi)|^2 + |\widehat{a}(\xi+\pi)|^2 \leq 1$ can be used to construct a complex tight framelet filter bank.

One possible shortcoming of the tensor product complex tight framelets TP-$\mathbb{C}$TF$_n$ considered in this paper is that the complex tight framelet filter banks do not have compact support in the space/time domain, which is one of the most desirable properties in wavelet analysis. One may suspect that it may be difficult to have TP-$\mathbb{C}$TF$_n$ with finitely supported filters. Fortunately, due to recent developments on one-dimensional complex tight framelet filter banks, finitely supported complex tight framelet filter banks with or without symmetry

have been well studied in [20, 21] and references therein. It turns out that it is quite flexible to construct finitely supported tensor product complex tight framelet filter banks with directionality from any low-pass filter a satisfying $|\widehat{a}(\xi)|^2 + |\widehat{a}(\xi+\pi)|^2 \le 1$, which is a necessary condition for constructing tight framelet filter banks. For construction of compactly supported tensor product complex tight framelets TP-$\mathbb{C}\mathrm{TF}_3$, this has been fully developed in [23]. We shall report elsewhere the detailed construction of compactly supported tensor product complex tight framelets TP-$\mathbb{C}\mathrm{TF}_n$ for any integer $n \ge 3$ and their performance for certain applications.

Acknowledgments. The authors would like to thank the anonymous referees for pointing out several related references and for their valuable suggestions which improved the presentation of the paper. The authors also thank W.-Q. Lim and X. Zhuang for providing us the test images of Lena and Barbara used in [27, 28].

REFERENCES

[1] I. Bayram and I. W. Selesnick, *On the dual-tree complex wavelet packet and M-band transforms*, IEEE Trans. Signal Process., 56 (2008), pp. 2298–2310.
[2] E. Candès, L. Demanet, D. Donoho, and L. X. Ying, *Fast discrete curvelet transforms*, Multiscale Model. Simul., 5 (2006), pp. 861–899.
[3] R. Chan, S. D. Riemenschneider, L. Shen, and Z. Shen, *Tight frame: An efficient way for high-resolution image reconstruction*, Appl. Comput. Harmon. Anal., 17 (2004), pp. 91–115.
[4] C. Chaux, L. Duval, and J.-C. Pesquet, *Image analysis using a dual-tree M-band wavelet transform*, IEEE Trans. Image Process., 15 (2006), pp. 2397–2412.
[5] I. Daubechies, *Ten Lectures on Wavelets*, CBMS-NSF Regional Conf. Ser. in Appl. Math. 61, SIAM, Philadelphia, 1992.
[6] I. Daubechies, B. Han, A. Ron, and Z. Shen, *Framelets: MRA-based constructions of wavelet frames*, Appl. Comput. Harmon. Anal., 14 (2003), pp. 1–46.
[7] M. N. Do and M. Vetterli, *Contourlets*, in Beyond Wavelets, G. V. Welland, ed., Academic Press, San Diego, CA, 2008.
[8] G. Easley, D. Labate, and F. Colonna, *Shearlet-based total variation diffusion for denoising*, IEEE Trans. Image Process., 18 (2009), pp. 260–268.
[9] G. Easley, D. Labate, and W. Lim, *Sparse directional image representations using the discrete shearlet transform*, Appl. Comput. Harmon. Anal., 25 (2008), pp. 25–46.
[10] W. T. Freeman and E. H. Adelson, *The design and use of steerable filters*, IEEE Trans. Pattern Anal. Mach. Intell., 13 (1991), pp. 891–906.
[11] B. Goossens, A. Pižurica, and W. Philips, *A filter design technique for improving the directional selectivity of the first scale of the dual-tree complex wavelet transform*, in Proceedings of the 16th IEEE International Conference on Image Processing (ICIP), 2009, pp. 3805–3808.
[12] K. Guo and D. Labate, *The construction of smooth Parseval frames of shearlets*, Math. Model. Nat. Phenom., 8 (2013), pp. 82–105.
[13] B. Han, *On dual wavelet tight frames*, Appl. Comput. Harmon. Anal., 4 (1997), pp. 380–413.
[14] B. Han, *Symmetric orthonormal scaling functions and wavelets with dilation factor* 4, Adv. Comput. Math., 8 (1998), pp. 221–247.
[15] B. Han, *Matrix extension with symmetry and applications to symmetric orthonormal complex M-wavelets*, J. Fourier Anal. Appl., 15 (2009), pp. 684–705.
[16] B. Han, *Symmetric orthonormal complex wavelets with masks of arbitrarily high linear-phase moments and sum rules*, Adv. Comput. Math., 32 (2010), pp. 209–237.
[17] B. Han, *Symmetric orthogonal filters and wavelets with linear-phase moments*, J. Comput. Appl. Math., 236 (2011), pp. 482–503.

[18] B. Han, *Nonhomogeneous wavelet systems in high dimensions*, Appl. Comput. Harmon. Anal., 32 (2012), pp. 169–196.
[19] B. Han, *Properties of discrete framelet transforms*, Math. Model. Nat. Phenom., 8 (2013), pp. 18–47.
[20] B. Han, *Matrix splitting with symmetry and symmetric tight framelet filter banks with two high-pass filters*, Appl. Comput. Harmon. Anal., 35 (2013), pp. 200–227.
[21] B. Han, *Symmetric tight framelet filter banks with three high-pass filters*, Appl. Comput. Harmon. Anal., to appear; available online from http://dx.doi.org/10.1016/j.acha.2013.11.001.
[22] B. Han, G. Kutyniok, and Z. Shen, *Adaptive multiresolution analysis structures and shearlet systems*, SIAM J. Numer. Anal., 49 (2011), pp. 1921–1946.
[23] B. Han, Q. Mo, and Z. Zhao, *Compactly Supported Tensor Product Complex Tight Framelets with Directionality*, preprint, arXiv:1307.2599, 2013.
[24] N. G. Kingsbury, *Image processing with complex wavelets*, Phil. Trans. R. Soc. Lond. A, 357 (1999), pp. 2543–2560.
[25] N. G. Kingsbury, *Complex wavelets for shift invariant analysis and filtering of signals*, Appl. Comput. Harmon. Anal., 10 (2001), pp. 234–253.
[26] G. Kutyniok and D. Labate, *Shearlets: Multiscale Analysis for Multivariate Data*, Birkhäuser/ Springer, New York, 2012.
[27] G. Kutyniok, M. Shahram, and X. Zhuang, *ShearLab: A rational design of a digital parabolic scaling algorithm*, SIAM J. Imaging Sci., 5 (2012), pp. 1291–1332.
[28] W.-Q. Lim, *Nonseparable shearlet transform*, IEEE Trans. Image Process., 22 (2013), pp. 2056–2065.
[29] J.-M. Lina and M. Mayrand, *Complex Daubechies wavelets*, Appl. Comput. Harmon. Anal., 2 (1995), pp. 219–229.
[30] J. Portilla, V. Strela, M. J. Wainwright, and E. P. Simoncelli, *Image denoising using scale mixtures of Gaussians in the wavelet domain*, IEEE Trans. Image Process., 12 (2003), pp. 1338–1351.
[31] A. Ron and Z. Shen, *Affine systems in $L_2(\mathbb{R}^d)$: The analysis of the analysis operator*, J. Funct. Anal., 148 (1997), pp. 408–447.
[32] I. W. Selesnick, *Smooth wavelet tight frames with zero moments*, Appl. Comput. Harmon. Anal., 10 (2001), pp. 163–181.
[33] I. W. Selesnick, *The design of approximate Hilbert transform pairs of wavelet bases*, IEEE Trans. Signal Process., 50 (2002), pp. 1144–1152.
[34] I. W. Selesnick, R. G. Baraniuk, and N. G. Kingsbury, *The dual-tree complex wavelet transform*, IEEE Signal Process. Mag., 22 (2005), pp. 123–151.
[35] L. Sendur and I. W. Selesnick, *Bivariate shrinkage functions for wavelet-based denoising exploiting interscale dependency*, IEEE Trans. Signal Process., 50 (2002), pp. 2744–2756.
[36] L. Sendur and I. W. Selesnick, *Bivariate shrinkage with local variance estimation*, IEEE Signal Process. Lett., 9 (2002), pp. 438–441.
[37] Z. Shen, *Wavelet frames and image restorations*, in Proceedings of the International Congress of Mathematicians (ICM), Vol. IV, New Delhi, 2010, pp. 2834–2863.
[38] M. Unser and D. Van De Ville, *Wavelet steerability and the higher-order Riesz transform*, IEEE Trans. Image Process., 19 (2010), pp. 636–652.
[39] R. van Spaendonck, T. Blu, R. Baraniuk, and M. Vetterli, *Orthogonal Hilbert transform filter banks and wavelets*, in Proceedings of the IEEE International Conference on Acoustics, Speech, and Signal Processing (ICASSP), Vol. 6, 2003, pp. 505–508.
[40] L. Wei and T. Blu, *A new non-redundant complex Hilbert wavelet transforms*, in Proceedings of the IEEE Statistical Signal Processing Workshop (SSP), 2012, pp. 652–655.